AFIT/GAE/ENY/93D-1

STATIC FRACTURE BEHAVIOR OF A CERAMIC MATRIX COMPOSITE AT ELEVATED TEMPERATURES

Thesis

David M. Agins, Captain, USAF

AFIT/GAE/ENY/93D-1

The views expressed in this thesis are those of the author and do not reflect the official policy or position of the Department of Defense or the U. S. Government.

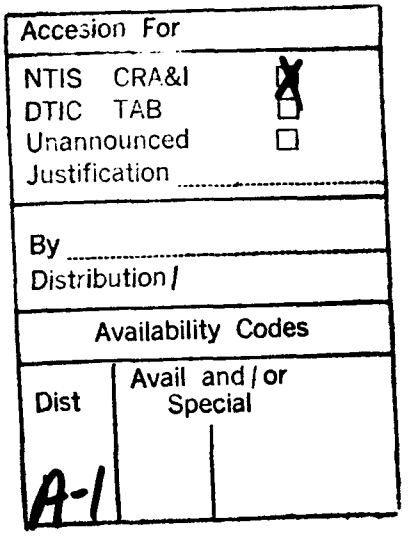

AFIT/GAE/ENY/93D-1

STATIC FRACTURE BEHAVIOR OF A CERAMIC MATRIX COMPOSITE AT ELEVATED TEMPERATURES

THESIS

Presented to the Faculty of the Graduate School of Engineering of the Air Force Institute of Technology Air University In Partial Fulfillment of the Requirements for the Degree of Master of Science in Aeronautical Engineering

David M. Agins
Captain, USAF

December 1993

Preface

The purpose of this study was to investigate the damage progression and failure modes of a ceramic matrix composite (Nicalon/CAS) when subjected to a static tensile load at elevated temperatures. This material is being studied for possible high temperature applications, including gas turbine engines and hypersonic airframes.

Extensive testing has been done on Nicalon/CAS at room temperature. Previous studies at elevated temperature have shown a significant drop in material properties and changes in failure modes of this material at 800^{o} C. This drop has been attributed to oxidation of the silicon carbide fibers. Understanding the change in static fracture behavior of this material as a result of this oxidation is important in evaluating its application to systems which would operate in such an environment. This research study is an attempt in this direction.

I would like to thank my thesis advisor, Dr. Shankar Mall, for his patience and guidance in conducting this study, lab technician Mark Derriso for his assistance and support, and Dr. Walter Jones, AFOSR/NA, for sponsoring this study. I would also like to thank my friends and classmates for their support and encouragement.

Table of Contents

List of Figures

List of Tables

Abstract

This study investigated systematically the damage initiation, damage progression, and failure modes of a ceramic matrix composite, Nicalon/CAS, when loaded in tension at elevated temperatures in the presence of air. A cross-ply lay-up, $[0/90]_{2S}$, was studied. The primary means of analysis were stress-strain data taken during monotonic tests to failure, and incremental load tests, also to failure, and crack density assessment. Testing was conducted at room temperature, 700° C, and 850° C. These temperatures were chosen as a result of previous studies that indicated a change in its behavior at 800° C. The stress-strain response was consistent for monotonic and incremental loading, except for a decrease in failure load at the elevated temperatures. Initial damage progression was also consistent, but the damage leading to failure and the final failure mode at 850° C were different due to the oxidation of the silicon carbide fibers. The oxidation created a brittle interface between the fiber and matrix, which resulted in an increase in fiber pull-out at the failure surface. Thermal cycling tests were also conducted to determine the effect of the heating and cooling necessary to take replicas during the incremental load tests. No noticeable effect of this thermal cycling on damage mechanisms was found.

1. Introduction

Composite materials have seen a significant amount of development in recent years. By offering lower weight, increased strength, and structural tailoring, they have seen widespread application. The continuing need for more efficient systems, as well as increased tolerance for hostile environments, has led to development of a wide variety of composites. One type that is being investigated for high temperature applications is ceramic matrix composites (CMC). Ceramics have been used in the past for high temperature applications, but their low fracture toughness has limited their use. By reinforcing ceramics with high strength fibers their toughness can be improved.

The primary damage mode of continuous fiber reinforced composite laminates is transverse matrix cracking. As a laminate is subjected to a monotonically increasing load, the number of transverse cracks increases until a saturation level is reached. The load is then transferred to the fibers until the material fails. A number of studies have been conducted to establish the mechanical properties and damage modes of CMCs at room temperature. Very little research has been done at elevated temperatures, which is needed due to the projected applications for these materials.

The purpose of this study is to investigate systematically damage initiation, damage progression, and failure modes of a model CMC, Nicalon/CAS, when loaded in tension at elevated temperatures in the presence of air. For this purpose, tests were conducted to determine the stress-strain response and material properties during monotonic and incremental load tests to failure. During the incremental tests, replicas were taken so that damage progression could be recorded through changes in crack density. Tests were conducted at room temperature, 700° C, and 850° C. These temperatures were chosen to provide a basis to investigate temperature effects. The room temperature response, which has been studied in the past, verifies the consistency of the material response of this study with previous studies. Previous elevated temperature testing of this CMC indicates a change in its response at approximately 800° C. Therefore, test temperatures of 700° and 850° C were chosen to determine the material response before and after this anticipated change. Thermal cycling tests were also conducted to determine the effect of the heating and cooling cycles necessary to take replicas during the incremental load tests.

2. Background

2.1. Introduction

Ceramic matrix composites (CMCs) have been developed and studied as a result of the demand for high temperature materials. Possible applications of CMCs include gas turbines and hypersonic airframes. They offer low density, high specific strength, and high temperature capabilities. Fiber-reinforced CMCs offer improvements over normal ceramics, such as non-brittle failure behavior, and increased strength and toughness. Nicalon/CAS is a CMC composed of Nicalon (silicon carbide) fibers and calcium aluminosilicate glass-ceramic matrix. Most of the previous research on Nicalon/CAS has been conducted at room temperature (1:215-222, 2:2851-2858, 3:109-131, 4:1-11, 5:613-618, 6). The high temperature testing, that has been reported, involved the investigation of the degradation of the material properties which occurred at temperatures above 800° C, and this was found to only take place in the presence of oxygen (7:136-151, 8, 9:C248-251, 10:33-51, 11:1537-1555).

Previous testing, including monotonic and cyclic tension tests of $[0/90]_{2s}$ Nicalon/CAS at room temperature and 815° C, has attributed this decrease in performance to embrittlement of the fiber/matrix interface (7:136-151). The purpose of this study is to characterize the damage

mechanisms and failure related to this degradation. Material properties and damage mechanisms were studied at room temperature, 700° C, and 850° C. A related study investigated the embrittlement behavior of SiC fiber-reinforced LAS and BMAS glass-ceramic composites during flexural testing in air (10:33-51). Although the test methodology is not directly applicable to this study, their results are useful in understanding the oxidation and embrittlement behavior of the fiber/matrix interface.

2.2. Room Temperature

Several room temperature tests have been conducted on unidirectional and cross-ply ceramic matrix composites to determine material properties and damage characteristics, and compare experimental results with theoretical predictions (1:215-222, 3:109-131, 4:1-11). These studies have shown that in cross-ply laminates initial damage is transverse cracking in the 90° plies, which then increases with increased load, followed by matrix cracks with fiber bridging in the 0° plies. Damage was found to be predominantly random matrix microcracking and fiber/matrix debonding, without delamination. The strain of crack initiation and crack density of 90° plies increased as the ply thickness decreased.

Mall and Kim investigated the failure mechanisms and mechanical behavior of Nicalon/CAS under static tension at room temperature. Moduli and poisson's ratio were found to match values predicted by classical laminated plate theory, but first ply failure and ultimate strength were not. The first ply failure prediction was lower than the experimental value, and the predicted ultimate strength was higher than the experimental value (1:215-222). Zawada, Butkus, and Hartman investigated the behavior of unidirectional and crossply specimens. Two proportional limits were found, the first being due to extensive cracking in the 90° plies, the second due to the nonlinear behavior of the 0° plies (2:2851-2858).

Harris, Habib, and Cooke investigated the mechanical properties of unidirectional and cross-ply samples of Nicalon/CAS. Elastic properties in tension, compression, and shear were studied, as well as damage during monotonic and repeated loading. Both components of this CMC are brittle, with low failure strains (0.0015 for CAS, 0.014 for SiC), resulting in its performance being limited by matrix cracking. Stress-strain curves showed similar behavior - linear initial portion, a knee at a stress level indicating extensive damage to cross-plies, a second linear portion of decreased slope, and a third nonlinear portion of increased slope. Incremental load tests of unidirectional and $[0/90]_{3s}$ specimens were performed to assess the effect of

matrix cracking on mechanical response. As cracking increased under tensile loading, the elastic moduli fell. Evidence of saturation crack density (corresponding to no change in modulus) was also found (3:109-131).

2.3. Elevated Temperature

Rousseau investigated the performance of a cross-ply laminate, $[0/90]_{2s}$, at 20° and 815° C under monotonic and cyclic loading. Rousseau found that the primary variation in material properties from room temperature (20° C) and 815° C was a decrease in failure stress, as well as a variation in the fracture surface. The initial elastic modulus, initial damage stress, and matrix cracking yield stress were consistent. Damage was initiated by 90° ply degradation, followed by transverse matrix cracking in the 0° plies, and ended with nonlinear strain. At 815° C the behavior was characterized by embrittlement of the fiber/matrix interface. During processing, fibers leach excess carbon into the fiber/matrix interface, which can oxidize at temperatures above 450° C. The interface is transformed at temperatures above 800° C due to the loss of the carbon during oxidation, and results in an embrittled composite behavior. Debonding occurs after periodic transverse cracks have formed in the 0° matrix, leading to a low number of fiber breaks, resulting in linear-elastic loading of the fibers (7:136-151).

Lee studied the damage development and mechanical response of heat treated Nicalon/CAS. Changes in damage and failure modes were found to be directly related to the condition of the interface. Specimens were heat treated for 100 hours at 900°, 1000° and 1100° C, and tested and compared to room temperature specimens. The heat treated specimens demonstrated brittle matrix crack propagation and uneven fiber pullout over the fracture surface. The unevenness of the fiber pullout is due to oxidation progression as cracks form in the matrix, allowing oxygen to diffuse and debonding to occur (8).

Mah and Mendiratta investigated the thermomechanical degradation of LAS/SiC CMC in an oxidizing atmosphere. Flexure and tensile tests of unidirectional specimens were conducted at 900° C and 1000° C. The oxidation/degradation was found to be dependent on loading, and occurred very rapidly. Loading was required to open cracks, exposing the interior of the specimen to the oxidizing atmosphere. Tests were performed in a vacuum and argon environments, and did not show any variation in material properties or behavior from room temperature results. Tests in partial air environments (varying oxygen levels) showed the dependence of the oxidation/degradation on air (9:C248-251).

Stewart, Chyung, Taylor, and Cooper studied the embrittlement behavior of SiC fiber reinforced LAS and BMAS composites. Both materials showed a significant drop in

ultimate strength and toughness when tested at 800° - 1100° C in air. Based on inert environment tests by Prewo (12) and Mah (13:245-260), which indicated that air, and more specifically, oxygen, is responsible for the degradation, tests in an inert environment were conducted, and showed no degradation in material properties. Flexural tests were conducted at room temperature and 100° increments from 700° - 1100° C. At room temperature fiber debonding/fiber pullout was present in the failure surface. The interface between the fiber and matrix was examined. In both materials an interface had formed, and is believed to be carbon, resulting from reactions between the fibers and matrix during processing. This carbon layer provides a weak interface for debonding and crack stoppage, resulting in a high toughness. Oxidation of this layer is believed to occur after the matrix has been cracked due to mechanical loading. Tests of heat-soaked specimens showed little to no property degradation, even though the material had microcracks as a result of processing. The oxidation is believed to either make the fibers brittle or form a strong interfacial bond (10:33-51).

3. Experimental Procedure

3.1. Introduction

This chapter presents the equipment and experimental methodology used in this study. The test equipment and its use are discussed, followed by the procedures used to prepare the specimens for testing. The final section is concerned with the actual procedures for the monotonic loading tests, incremental load tests, and temperature exposure tests.

3.2. Test Station

The test station consisted of four major components: material test equipment, heating and cooling equipment, control systems, and data acquisition systems.

The material test equipment included the test stand, hydraulic grips, and high temperature extensometer (see Figure 1). The test stand was the MTS 810 Material Test Station. This test stand has a maximum force capability of 100 kN that is applied by an integral hydraulic actuator. Alignment was checked during initial installation as well as prior to testing. The grips used were the MTS 647.02 hydraulic wedge grips, modified to incorporate cooling during high temperature tests. The cooling lines can be seen in Figure 1. A grip pressure of 6 MPa was used for the

tests. Prior to testing, the grips were checked for maximum temperature to ensure that the maximum allowable value of 177° C would not be exceeded. The maximum temperature reached in these tests was 89° C. The extensometer used for the tests was the MTS 632.65B-03 with quartz rods. The extensometer was calibrated for a 2.54 cm gage length prior to testing.

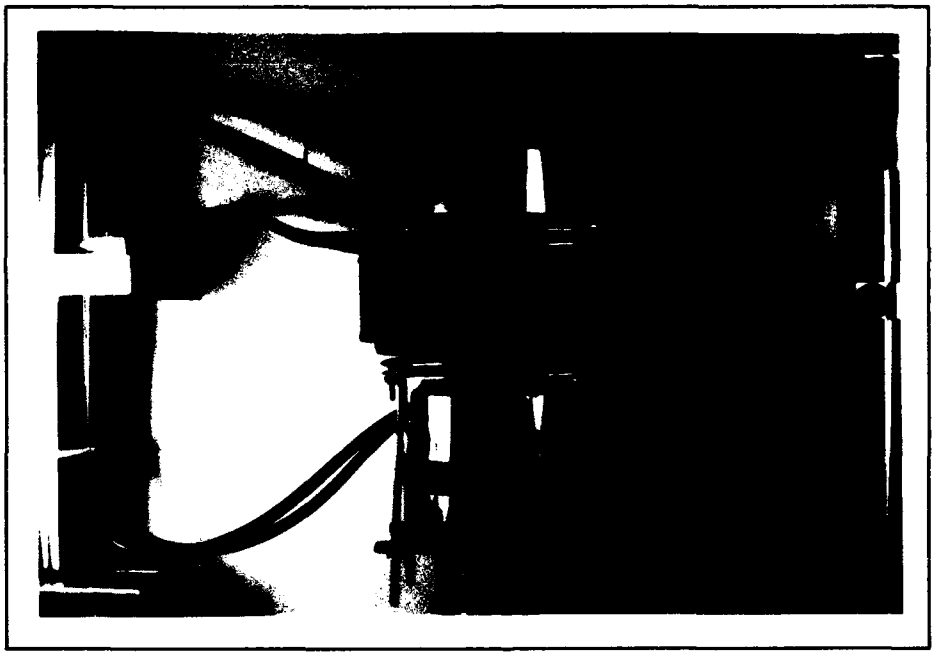

Figure 1. Material Test Equipment

Specimens were heated using two heat lamps equipped with quartz bulbs. Each lamp could hold up to four bulbs, but for these tests only two bulbs per lamp were sufficient.

Cooling was provided by a Neslab HX-75 refrigerated recirculation unit in a closed-loop system. This unit provided cooling water to the grips, extensometer mount, heat shields, and heat lamp assemblies. The heat shields were designed for these tests and provided additional protection for the grips as well as limited the heated zone of the specimen to the gage length. The heat shields and their cooling lines can be seen in Figure 1.

The test stand was controlled by an MTS 458.20 MicroConsole. Load control for the tests was provided by an MTS 458.11 DC Controller (with 8896 N load card). An MTS 458.13 AC Controller (with 12.7 cm displacement card) was used to provide additional control. Both control systems and cards were calibrated prior to testing as part of the test station's periodic maintenance. The heat lamps were controlled using Barber-Colman 560 temperature controllers. Heating and loading of the test specimens was controlled by a Zenith Z-386 personal computer, using the MATE software package. For the replica tests, a Wavetek Model 75 Waveform Generator was used to provide additional load control.

Data acquisition was conducted by the Zenith Z-386 using the Material Analysis and Test Environment (MATE) software package.

3.3. Specimen Preparation

Ceramic matrix composites are generally fabricated by a two-stage process. In the first stage, fibers are incorporated into an unconsolidated matrix, usually by the slurry infiltration process. The fiber tow is passed through a slurry tank containing the matrix powder, binder, and carrier liquid, wound on a drum, and allowed to dry. The tows are then cut, stacked, and hot pressed at 1200° C (14:51). Nicalon/CAS is a CMC made of Nicalon fibers (predominantly silicon carbide amorphous/crystalline fibers) made by the Nippon Carbon Company, and calcium-aluminosilicate glass-ceramic made by Corning Glass. For these tests, a $[0/90]_{2s}$ lay-up was used.

Test specimens were cut from a 15.3 cm x 15.3 cm x 0.3175 cm plate, with specimens having a width of 0.51 cm and a length of 15.3 cm. For replication tests, six specimens were ground, lapped, and polished using 68 micron (fine grind), 30 micron (rough polish), 12 micron (medium polish), and 6 micron (fine polish) diamond impregnated wheels, and 9, 6, 3, and 1 micron diamond suspensions and pastes. Optical inspection was used between these polishing stages to determine completion. All specimens had four aluminum (2020-0) tabs with approximate dimensions of 2.5 cm x 0.6 cm x 1.6 mm attached to the ends using epoxy (see Figure 2). The epoxy was cured at 71° C for 90 minutes in an oven. These tabs protected the specimens from the grips

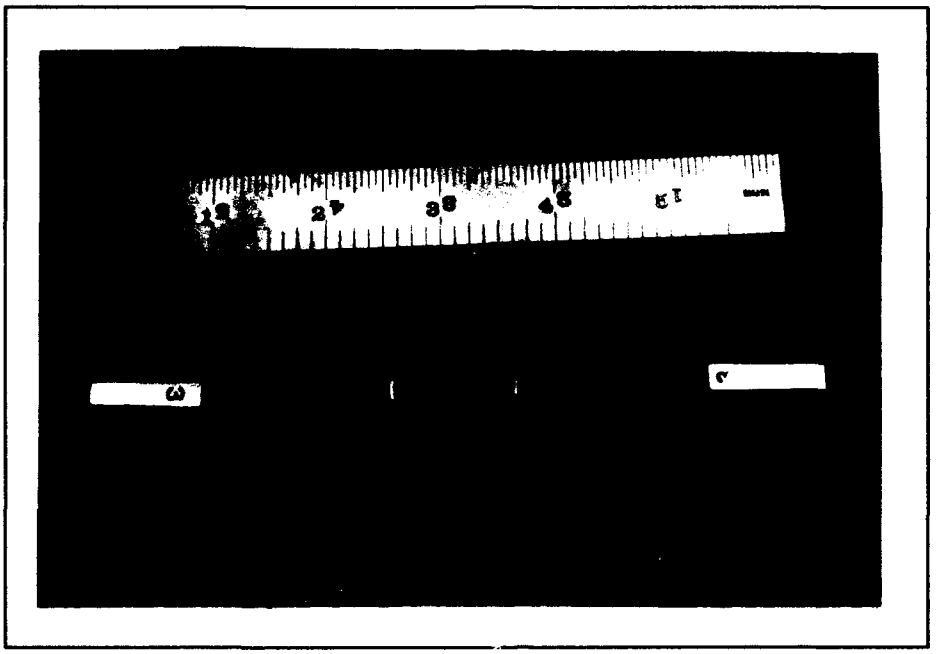

Figure 2. Specimen with Aluminum Tabs

and prevented crushing and surface damage. Specimens were mounted in the middle of the grips with the tabs completely in the grips and aligned with the integrated actuator using the specimen alignment tool (see Figures 3 and 4).

For the 700° C and 850° C tests, K-type thermocouples were attached to the surface of the specimens using 903 Green ceramic glue. The thermocouples were held in place against the specimen with 36 gage alumel wire (Figure 5) while the glue was applied and cured (Figure 6). The glue was cured using the heat lamps at 120° C for 120 minutes. The thermocouples were attached at points outside (above and below) of the 2.54 cm gage section (see Figure 7).

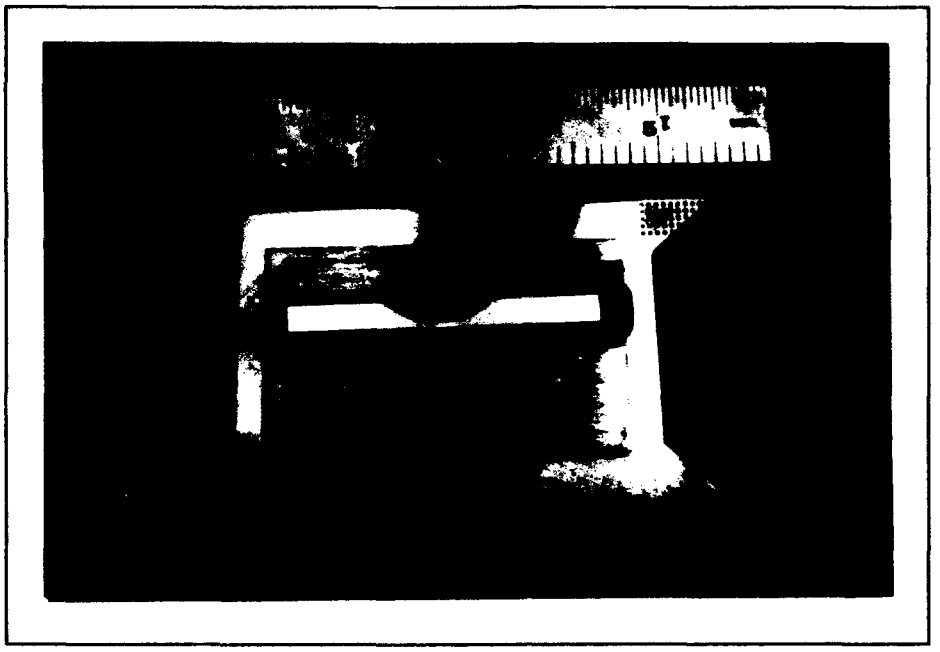

Figure 3. Specimen Alignment Tool

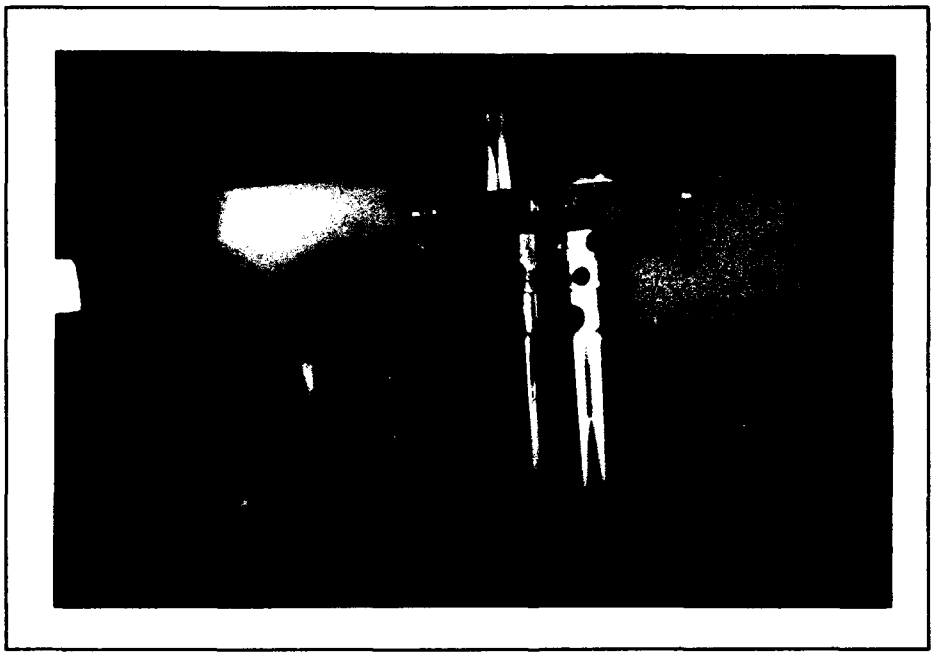

Figure 4. Checking Alignment of Integrated Actuator

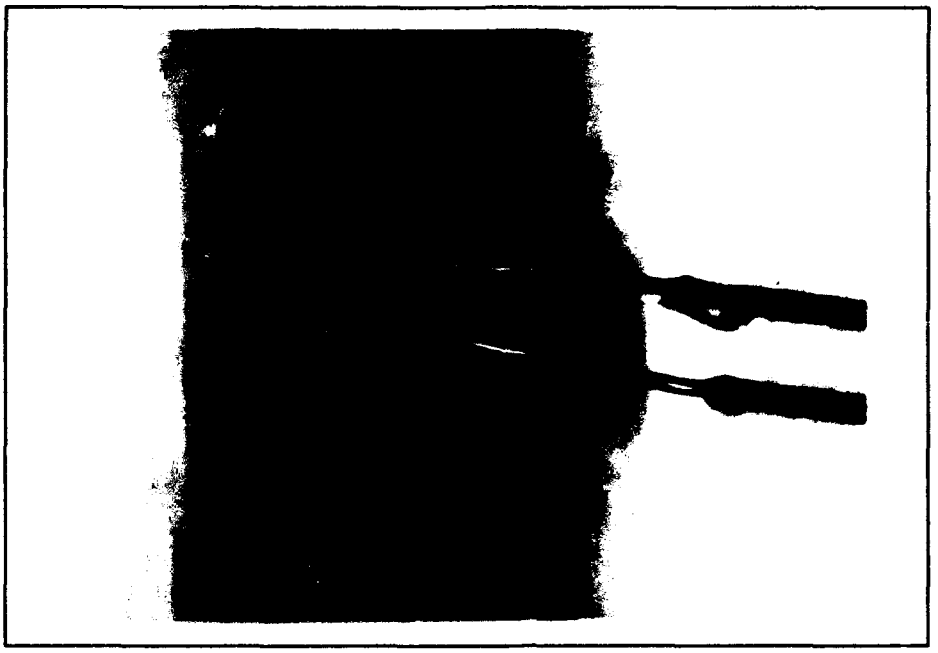

Figure 5. Thermocouple Attachment

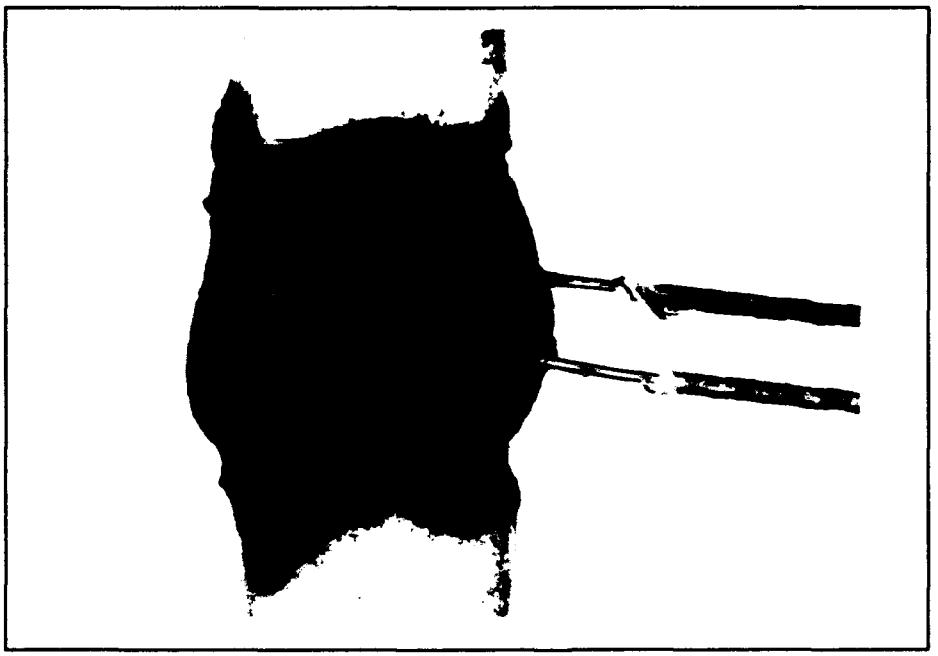

Figure 6. Thermocouple Attachment

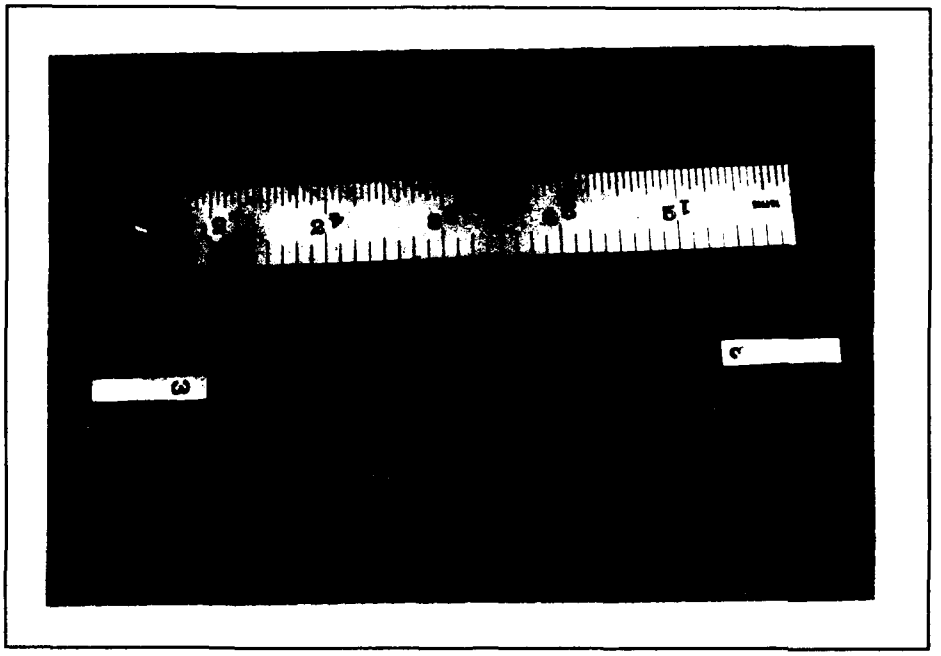

Figure 7. Specimen Prior to Thermocouple Attachment

The thermocouples were used to control the output of the heat lamps. Placing them above and below the gage section prevented them from interfering with the extensometer rods and ensure complete heating of the gage section (see Figure 8).

3.4. Test Procedure

All tests were conducted under load control, with a load rate of 1 MPa/sec. For the high temperature tests, a heating ramp time of 5 minutes was used to bring the specimen to the test temperature (Figure 9, points 1 and 2). The specimens were then soaked at the test temperature for

10 minutes to ensure complete heating of the specimen in the gage section (Figure 9, points 2 and 3). Loading was initiated after completion of the ten minute soak period.

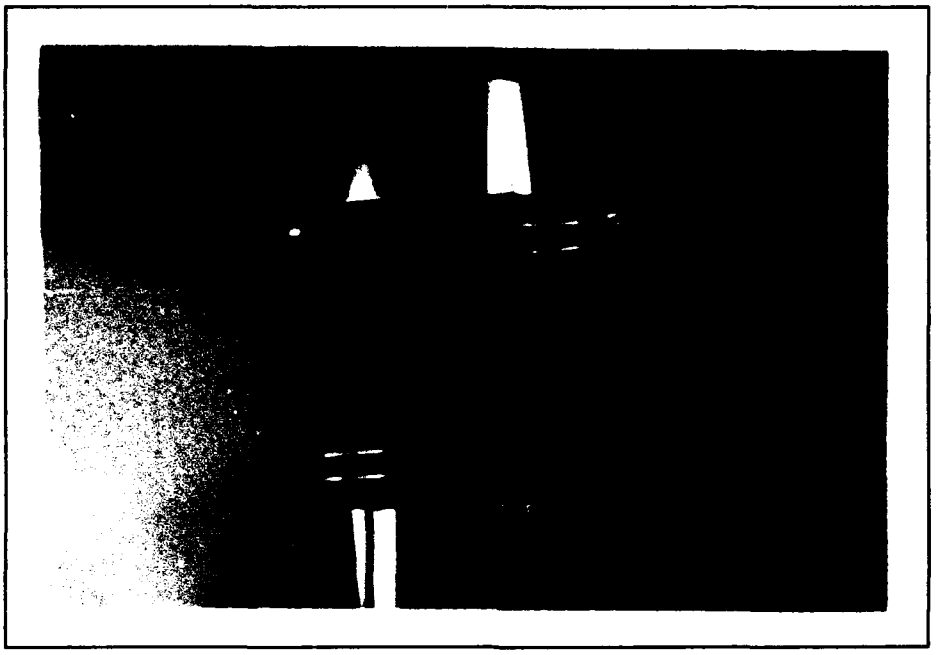

Figure 8. Thermocouple and Extensometer Position

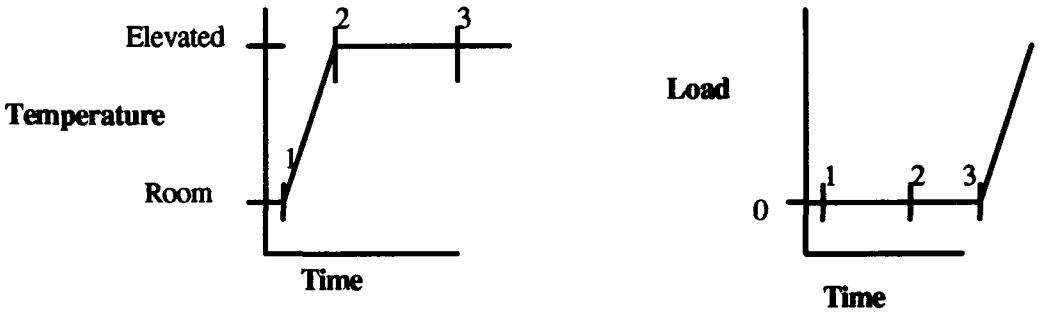

Figure 9. Temperature and Load Cycles (Monotonic)

The lamps to heat the specimens use quartz bulbs to generate heat. The lamp bodies are capable of holding up to four bulbs, but for these tests only two bulbs per lamp were required. Two lamps were used to heat the specimen, with the bulbs placed asymmetrically, corresponding to the location of the thermocouples. The thermocouple on the front of the specimen was below the gage section, so the front lamps were in the lower two mounts of the lamp body; the back thermocouple was above the gage section, so the rear lamps were in the upper mounts. The thermocouples provided temperature data to the lamp controllers which controlled power provided to the lamps. The offset position of the thermocouples and lamps, in addition to the ten minute soak time, provided uniform heating of the gage section. The positioning of the rear lamp is shown in Figure 10.

For the ultimate tests, the software package MATE (Material Analysis and Testing Environment), was used to control the test and record data. For the incremental tests, MATE was used to control the lamps, the PC DAS (digital acquisition system) utility module in MATE was used to record the data, and the Wavetek waveform generator was used to control the load signal and profile. The Wavetek produced a signal that peaked at 10 volts, so the span control on the load card was used to control the magnitude of the load. The load profile was a triangle wave set to

Figure 10. Positioning of Rear Lamp Assembly

load/unload at a rate of 1 MPa/sec. Only one period of the wave was used to load the specimen up to the desired level, and then return the load to zero. The frequency of the triangle was calculated for each load level, since it was dependent on the load rate and stress, σ. The frequency of the wave (f_W) was calculated by the formula $f_w = 1/T$, where the period $T = 2*\sigma/\text{load rate}$. This frequency was used to set the sample frequency (f_S) of the Wavetek, calculated by $f_s = f_w * \text{memory}/\text{cycles}$. Memory was 1000 data points, and cycles to memory was one. An oscilloscope was used to verify the output signals. The wave frequency and sample frequency were calculated for each load level, and the Wavetek was reset before each load cycle. The temperature and load profiles for two complete cycles are shown in Figure 11.

Loads 1 and 3 are incremental loads (increasing in magnitude with each cycle until failure) and loads 2 and 4 are replica load, which were the same for each cycle.

The load level for each increment was determined using the monotonic stress-strain response curve. Load magnitudes were chosen above and below each knee of the curve, and at regular intervals.

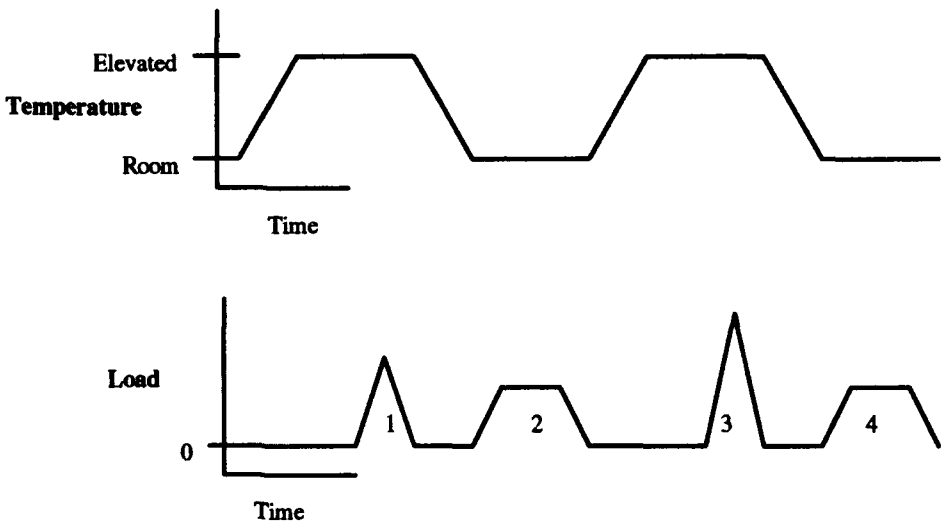

Figure 11. Temperature and Load Cycles (Incremental)

Replicas were taken using acetone and acetate film. The area to be replicated was swabbed with acetone, and the film was immediately pressed against it and held in place for 30 seconds. Optical inspection was used to confirm quality/resolution. An initial replica was taken to determine if a significant number of cracks existed (from

manufacturing or specimen preparation) and to provide a baseline for determining crack growth and progression.

Temperature exposure tests were conducted to determine if the heat cycles (ramp to test temperature, soak at test temperature, cool to room temperature) had any affect on damage or damage progression, and there was none, as discussed in the next chapter. Three tests were conducted, one at 700° C and two at 850° C. The tests were conducted in the same manner as the incremental load tests, the only difference being that the initial load was larger and no incremental loads were applied during the additional cycles. This resulted in an initial load and four cycles of heating, soaking, and cooling. For the 700° C test, the specimen was loaded to approximately 40% of its ultimate strength. This load value is beyond the first knee of the stress-strain curve, producing an observable amount of damage. Two tests were conducted at 850° C, one loaded to 40%, the other to 70% to determine if the extent and type of initial damage changed during the heat cycling. Since there was no change in damage in the 70% load test at 850° C, a 70% load test at 700° C was not performed. Replicas were taken to enable this assessment by measuring the crack density.

Crack densities were calculated by counting the number of cracks observed on a specimen's replica using an optical microscope. A baseline length of 5 mm was used, and the number of cracks were divided by this length to obtain an

average density per unit length, in this case, mm. Counts were made of each ply (0, 90, 0, 90/90, 0, 90, 0) and totals for the 0° and 90° plies were plotted versus the maximum strain for that cycle.

In summary, the following tests were performed: ultimate tests at room temperature, 700° C, and 850° C; incremental tests at room temperature, 700° C, and 850° C; temperature exposure tests at 700° C (one load level) and 850° C (two load levels).

4. Results

4.1. Introduction

This section includes the results and their analysis for the monotonic and incremental tests. The stress-strain response of the monotonic and incremental tests are presented and compared, followed by a discussion of the crack density results from the incremental tests. The damage progression, which was consistent in all cases, is presented next, followed by a discussion on the morphology of the failure surfaces.

4.2. Stress-Strain Response

4.2.1. Monotonic. The measured stress-strain relationships at the three temperatures, room temperature, 700° C, and 850° C, are shown in Figures 12, 13, and 14. A comparison of these curves shows similar behavior at all three temperatures. All three curves have an initial linear portion, two knees (labeled points A and B) separated by a second linear portion of decreased slope, followed by a nonlinear region prior to failure. Figure 15 shows the three curves plotted together to emphasize the similarities. For all three tests, the first knee occurs at a stress of approximately 40 MPa, and a strain between 0.0003 and 0.00035 mm/mm. The second knees occur between a stress of 105 and 120 MPa, and a strain between 0.0016 and 0.0018

mm/mm. An expanded view of the initial region of these curves, Figure 16, shows the similarities in the moduli over the elastic region for the three temperatures. The initial moduli are 129.2, 117.6, and 106.5 GPa (see Table 1). The initial moduli decrease as the test temperature increases, indicating a softening of the matrix. Failure stresses and strains also decrease as the temperature increases, Table 1. The room temperature results matches the corresponding results from Rousseau's previous study, and the 850° C results are close to Rousseau's data for 815° C (14:138).

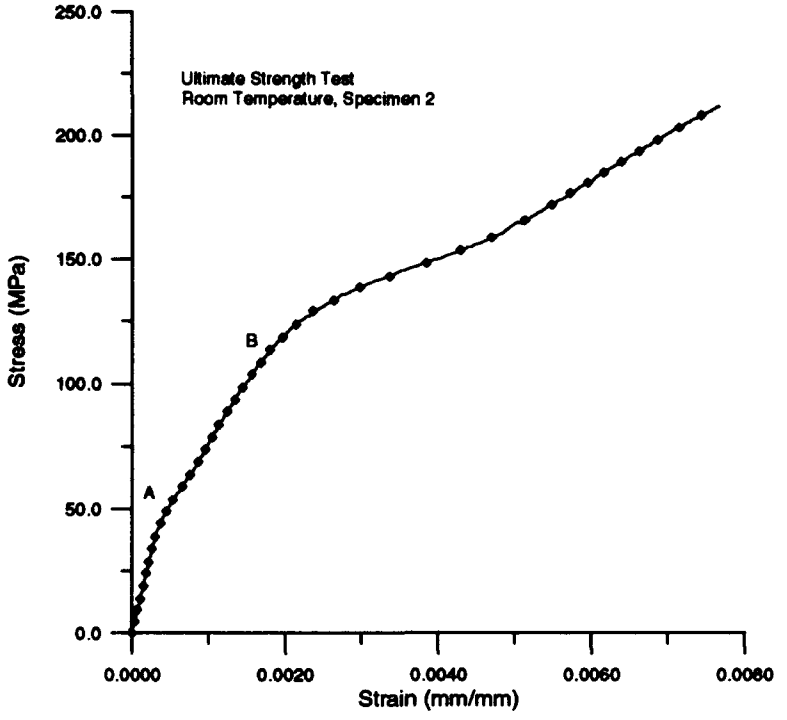

Figure 12. Stress-Strain Curve for Room Temperature Monotonic Test

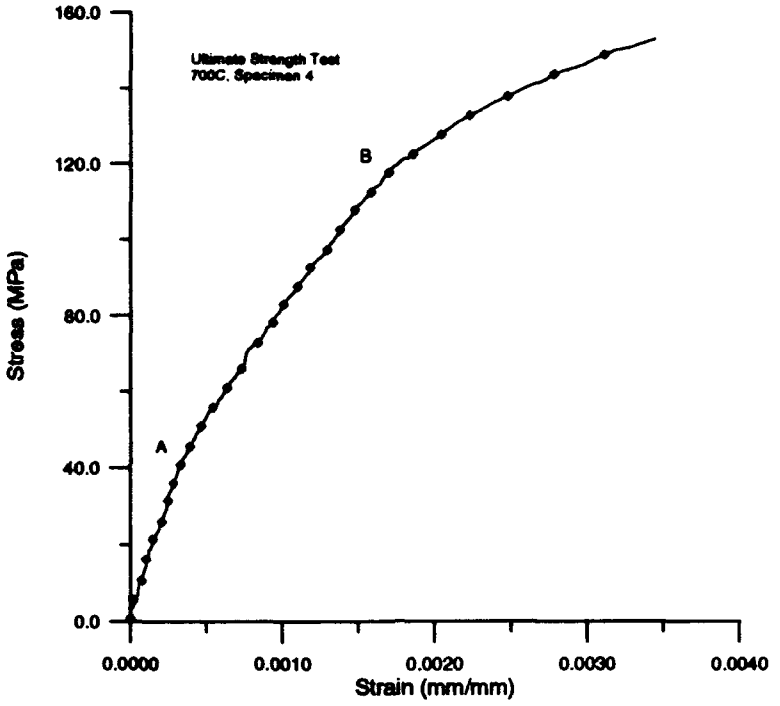

Figure 13. Stress-Strain Curve for 700° C Monotonic Test

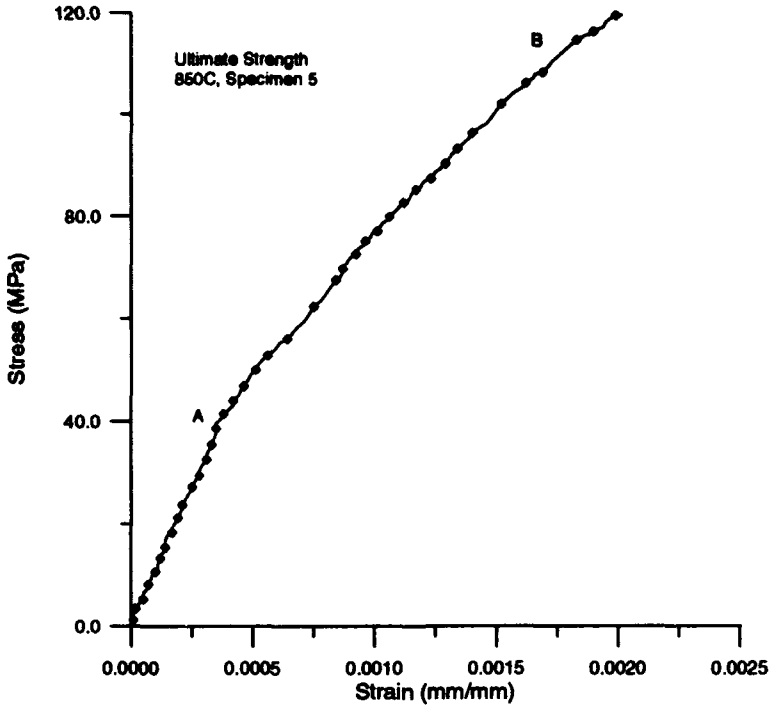

Figure 14. Stress-Strain Curve for 850° C Monotonic Test

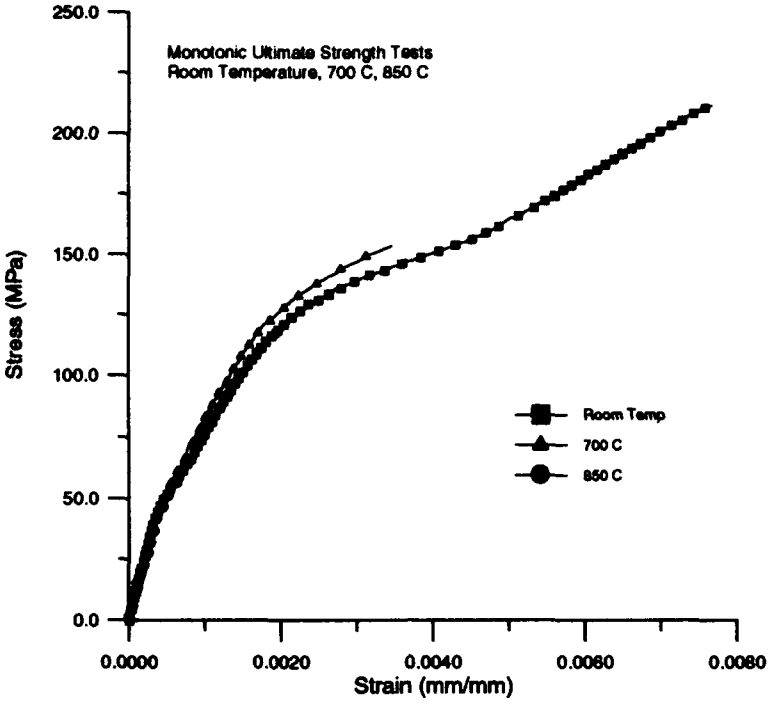

Figure 15. Stress-Strain Curves for Monotonic Tests

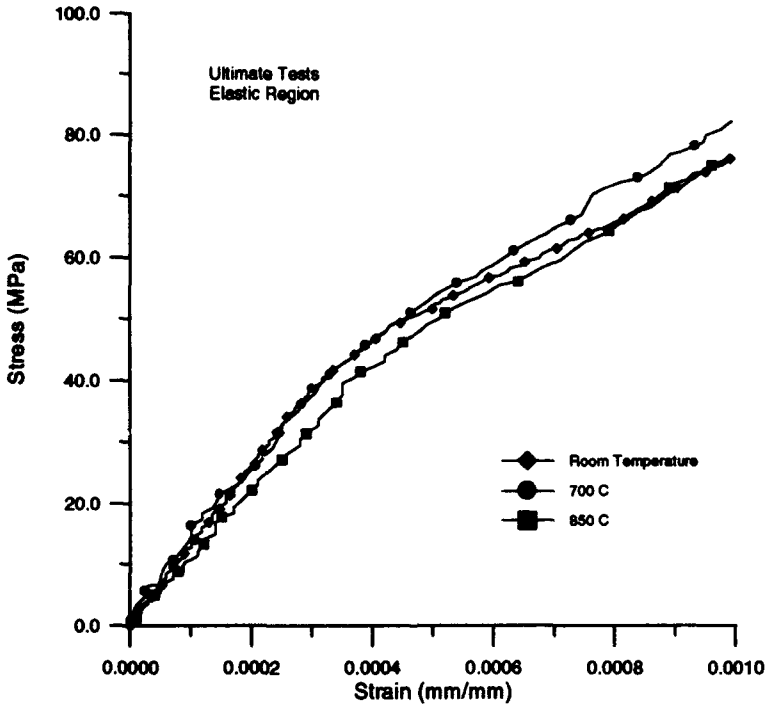

Figure 16. Initial Load Regions

Table 1. Summary of Monotonic Test Results

Temperature	Initial Moduli (GPa)	Failure Stress (MPa)	Failure Strain (mm/mm)	Source
Room Temperature	129.2	211.8	0.007649	Present Study
700° C	117.6	151.7	0.006435	
850° C	106.5	119.4	0.005268	
Room Temperature	123.5	228.4	----	Rousseau (14:138)
815° C	116.1	136.5	----	

4.2.2. Incremental Tests. The stress-strain response of the incremental load tests compared very well with the monotonic responses, as shown in Figures 17, 18, and 19. The initial and final load cycles, including failure, are shown along with the monotonic test stress-strain curve. In all cases the initial load curve was the same as the initial load region of the corresponding monotonic test, and the behavior of the cumulative incremental load curves mirrored that of the monotonic test. For all incremental loads, the moduli decreased as the number of load cycles increased, indicating increased damage with each cycle (see Table 2). The unloading moduli, normalized with respect to the initial loading moduli from the first incremental load, were used for this comparison. The unloading moduli were calculated using a linear approximation of the unloading portion of the

stress strain curve. The normalized unloading modulus versus strain relationship shows similar behavior at all three temperatures (see Figure 20). The room temperature results match with those found by Harris, Habib, and Cooke in the case of $[0/90]_{3s}$ under tension at room temperature (4:120).

Figure 17 shows the stress-strain relationship at room temperature for incremental loads. Here a greater amount of residual strain was observed than in the case of the higher temperature tests. During the higher temperature tests the incremental loading curves were closer together, and the residual strain was low, as shown in Figures 18 and 19.

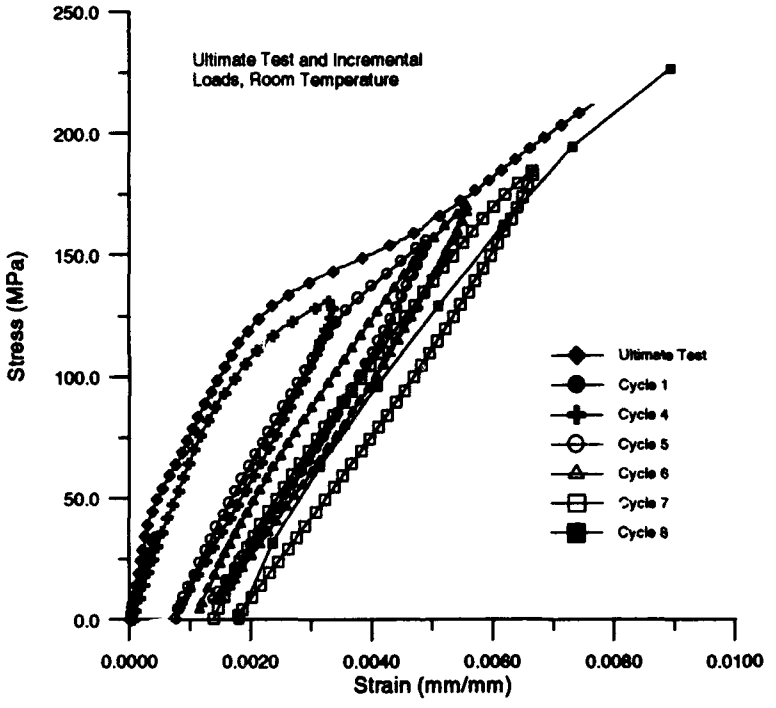

Figure 17. Incremental Load Comparison, Room Temperature

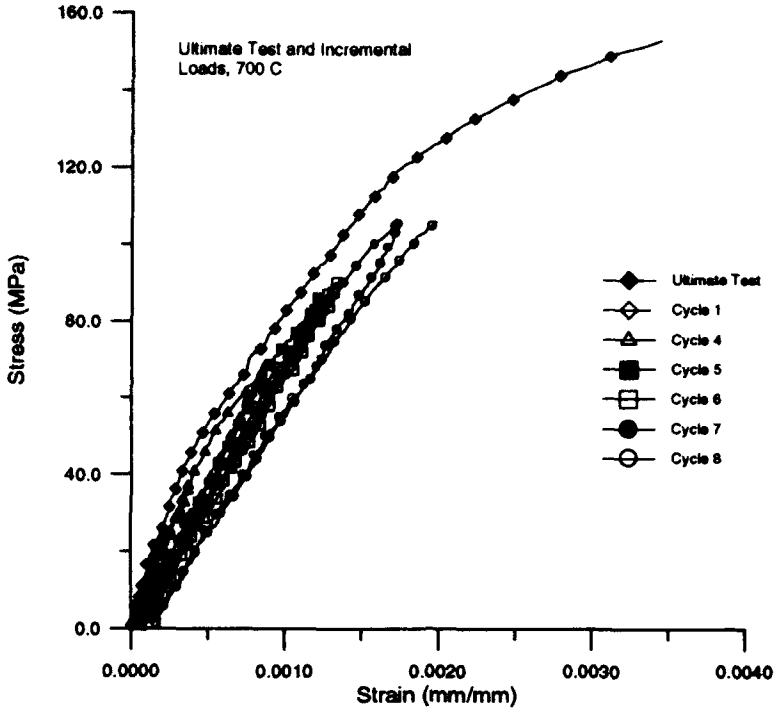

Figure 18. Incremental Load Comparison, 700° C

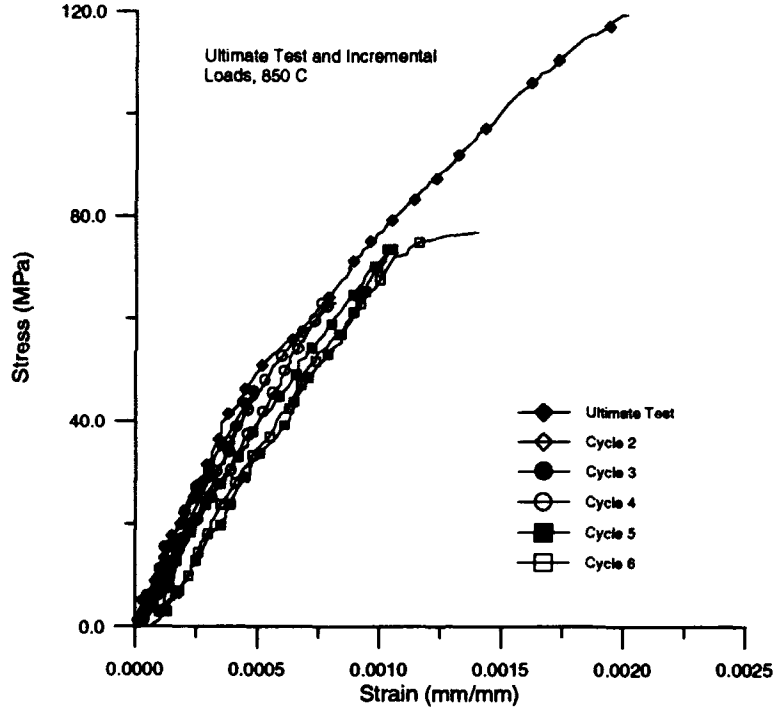

Figure 19. Incremental Load Comparison, 850° C

Table 2. Comparison of Unloading Moduli

Load Cycle	Normalized Modulus		
	Room Temp	700° C	850° C
1	0.9496	0.9973	0.9575
2	0.8982	0.8823	0.9430
3	0.7905	0.7440	0.8082
4	0.5368	0.6602	0.6569
5	0.4543	0.6281	0.6268
6	0.4306	0.5838	------
7	0.4198	------	------

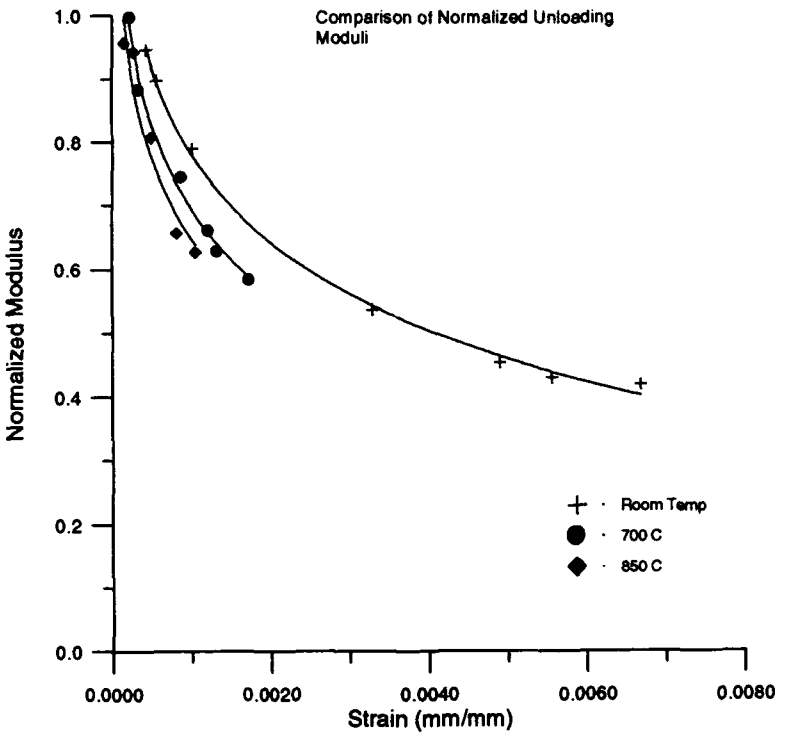

Figure 20. Normalized Moduli From Incremental Load Tests

4.3. Crack Density

The crack density from the tests conducted at incremental loads was used to confirm the change in modulus which indicated an increase in damage with increase in temperature, as well as to characterize the type and progression of damage. Crack densities were calculated by counting the number of cracks observed on a specimen's replica using an optical microscope. A baseline length of 5 mm was used, and the number of cracks were divided by this length to obtain an average density per unit length, in this case, mm. Counts were made of each ply (0, 90, 0, 90/90, 0, 90, 0) and totals from all the 0° and 90° plies were plotted as a function of the maximum strain to which the specimen was subjected.

Room temperature crack density demonstrates roll-off/ saturation for both 0° and 90° plies, as shown in Figure 21. A comparison of the crack density in the 0° plies (Figure 22) shows a distinct variation from room temperature to elevated temperatures. The room temperature crack density appears to reach a saturation level, while the 700° C and 850° C curves are still increasing. The comparison of crack density 90° plies (Figure 23) shows the same behavior.

4.4. Damage Progression

Damage initiates in the central 90° plies, which is the widest section among all the plies. This confirms the findings of Karandikar, Prashant, and Chou (4:4-5)

concerning initiation strain of transverse cracks. Their results showed that the crack initiation strain decreased as the ply thickness increased. Cracks initiated at voids or defects, then expanded to bridge the entire thickness of the ply. All cracks were assumed to be throughout the entire thickness of the specimen. The initial load cycle resulted in some cracks that spanned the entire laminate thickness. Crack spacing/density was found to be dependent on (or approximately equal to) laminate thickness, as found by Karandikar, Prashant, and Chou (4:4-5). The series of

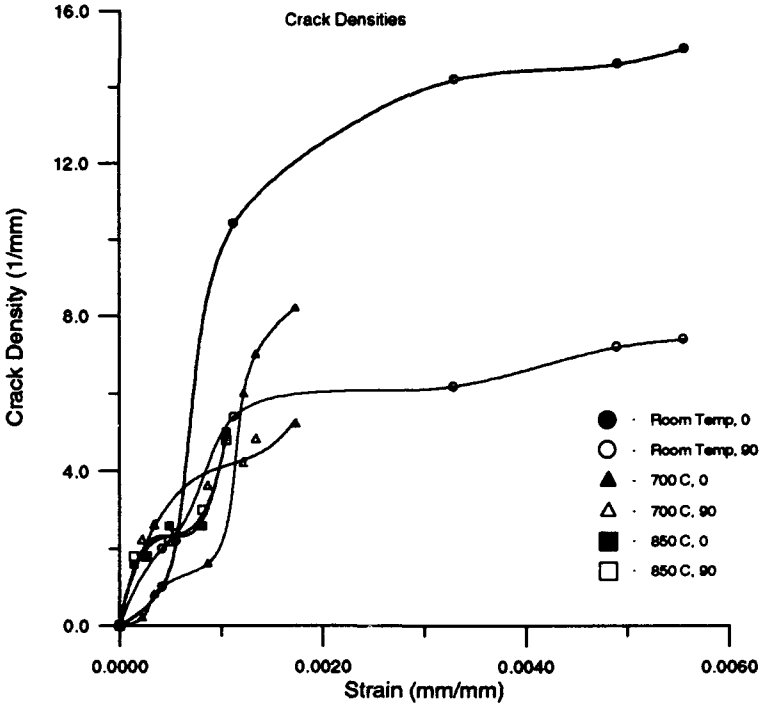

Figure 21. Crack Density Comparison

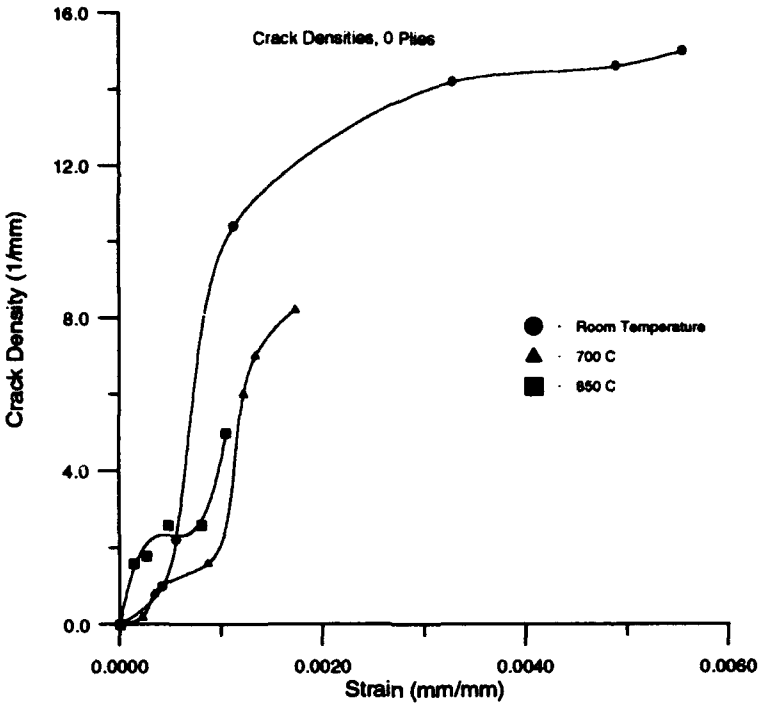

Figure 22. Crack Density Comparison in 0° Plies

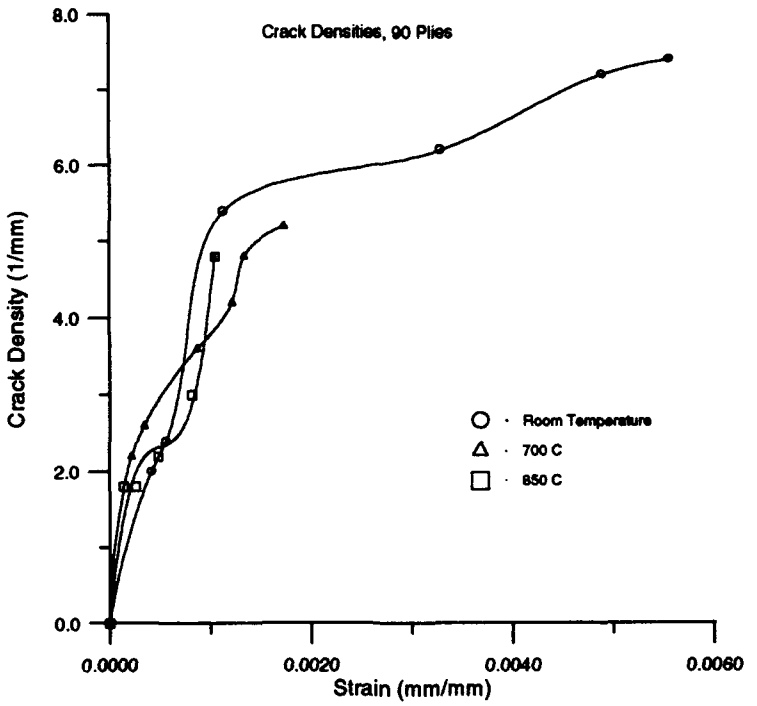

Figure 23. Crack Density Comparison in 90° Plies

replica photographs (Figures 24-39) shows the progression of damage after incremental loads were applied to specimens at the three test temperatures. The replicas were taken at room temperature with an applied 22.4 N load to make the cracks more detectable. In many cases the 0° ply cracks were extensions of cracks which originated in the 90° plies. The cracks in the 90° plies normally propagated to span the entire lamina, whereas the cracks in the 0° plies were shorter, originating in matrix rich regions, and propagated at a slower rate. This is expected since the fibers are perpendicular to the cracks and prevent/delay their progression. As shown in the final cycle replica

Figure 24. Room Temperature, ε = 0.000557, x32

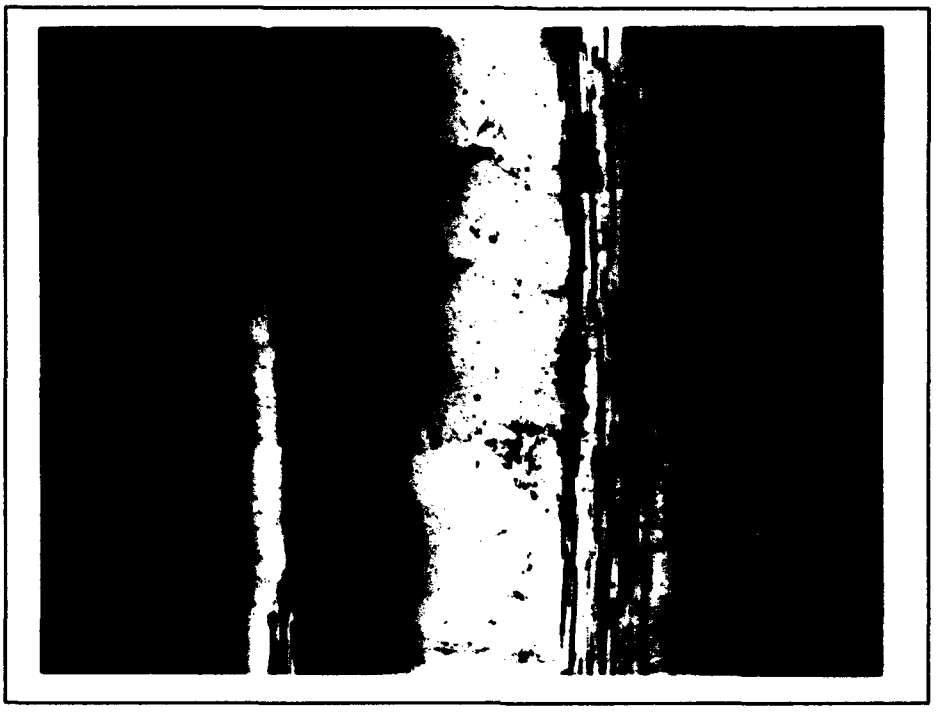

Figure 25. Room Temperature, ε = 0.00113, x32

Figure 26. Room Temperature, ε = 0.00329, x32

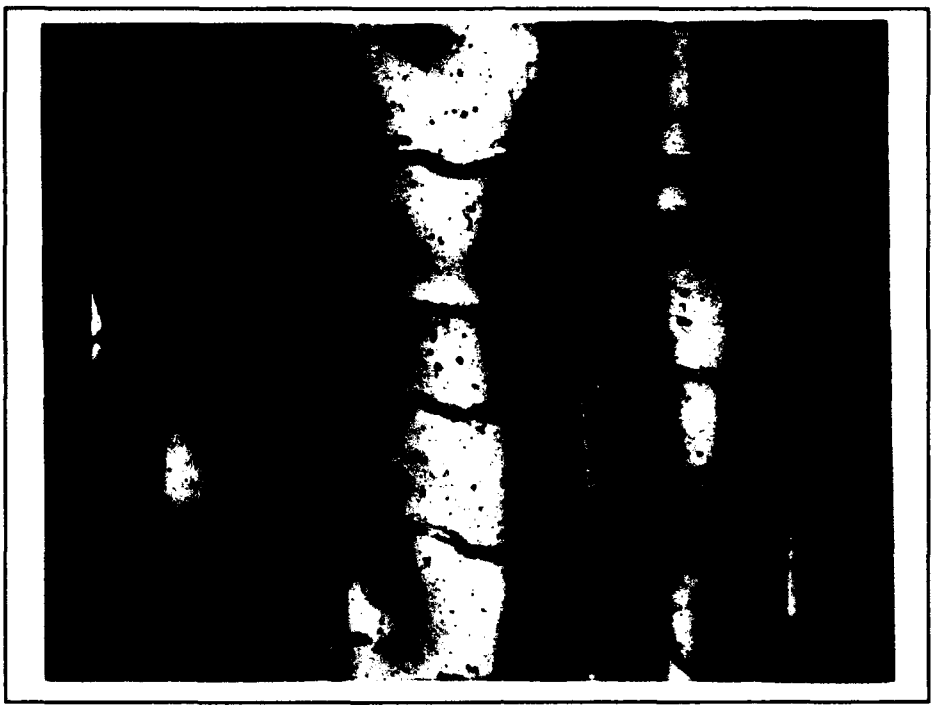

Figure 27. Room Temperature, ε = 0.00490, x32

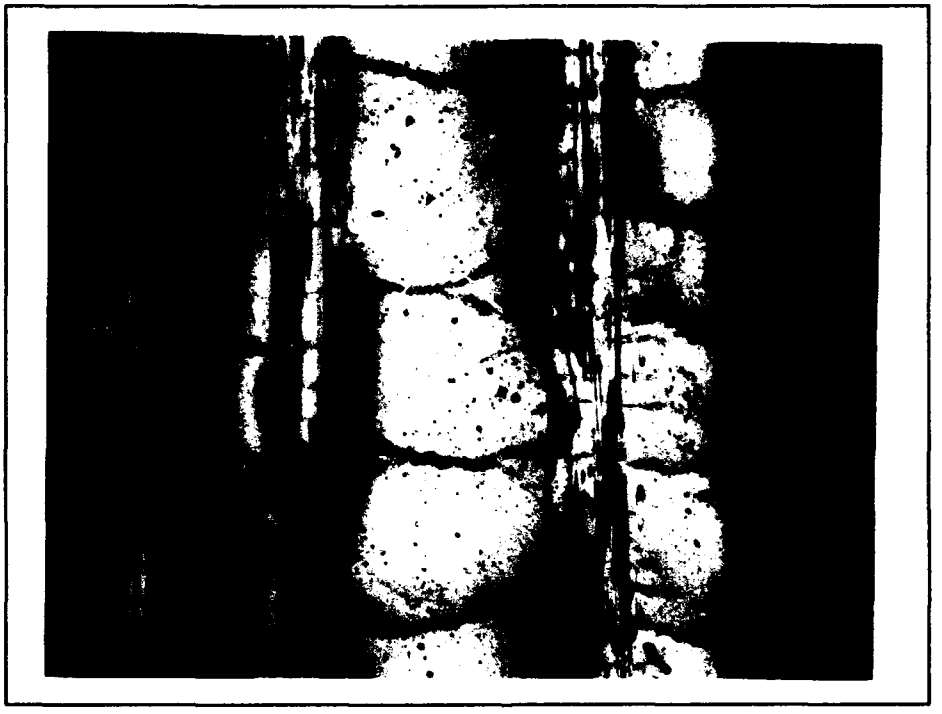

Figure 28. Room Temperature, ε = 0.00556, x32

Figure 29. Room Temperature, ε = 0.00668, x32

Figure 30. 700° C, ε = 0.000215, x32

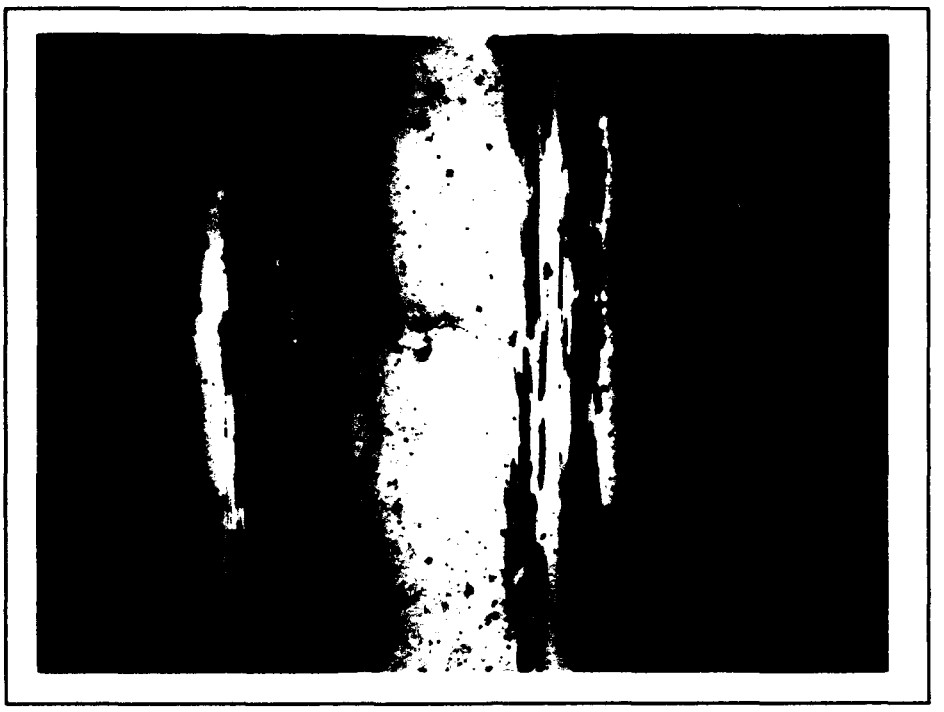

Figure 31. 700° C, ε = 0.000340, x32

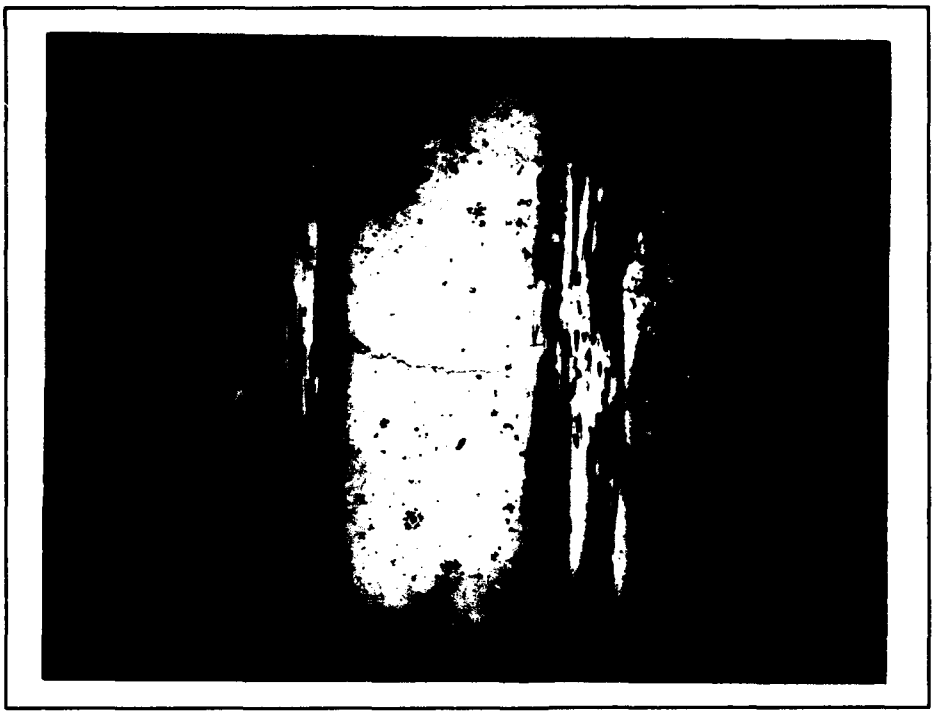

Figure 32. 700° C, ε = 0.00121, x32

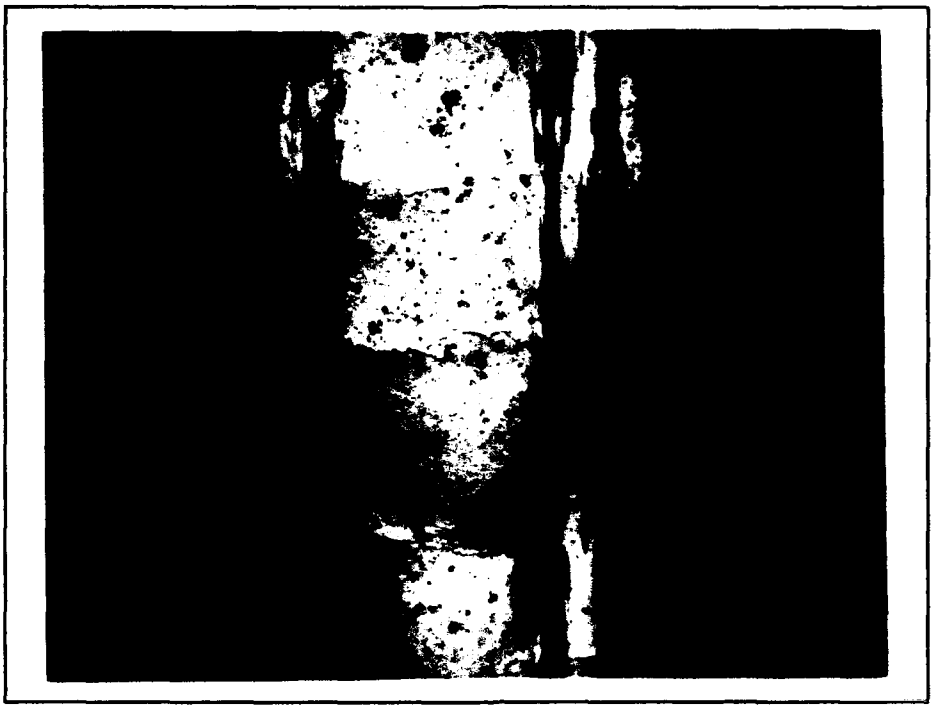

Figure 33. 700° C, ε = 0.00133, x32

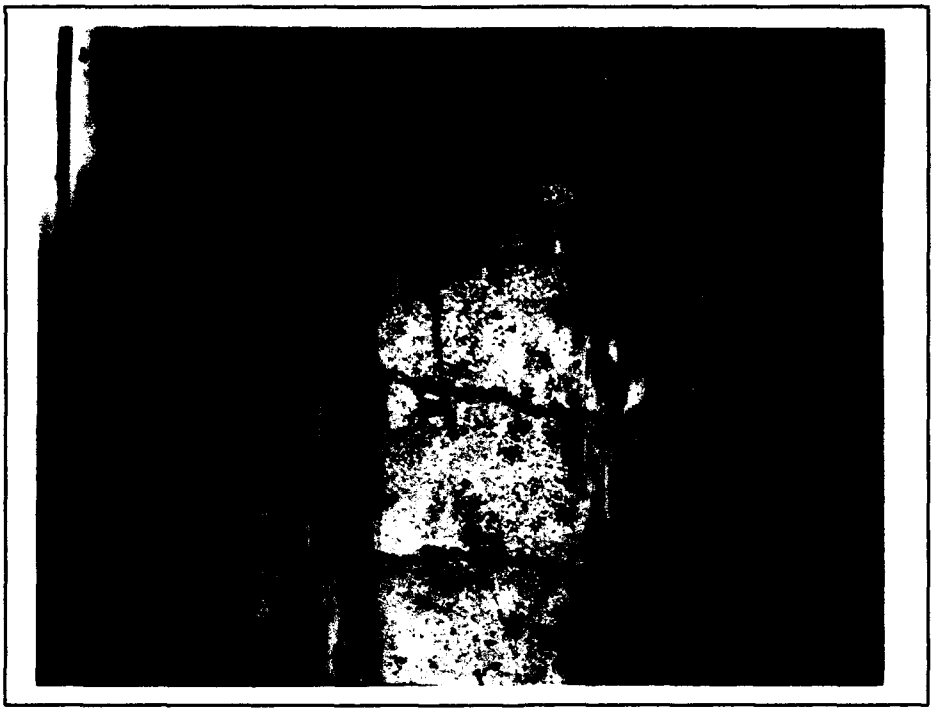

Figure 34. 700° C, ε = 0.00173, x32

Figure 35. 850° C, ε = 0.000135, x32

Figure 36. 850° C, ε = 0.000263, x32

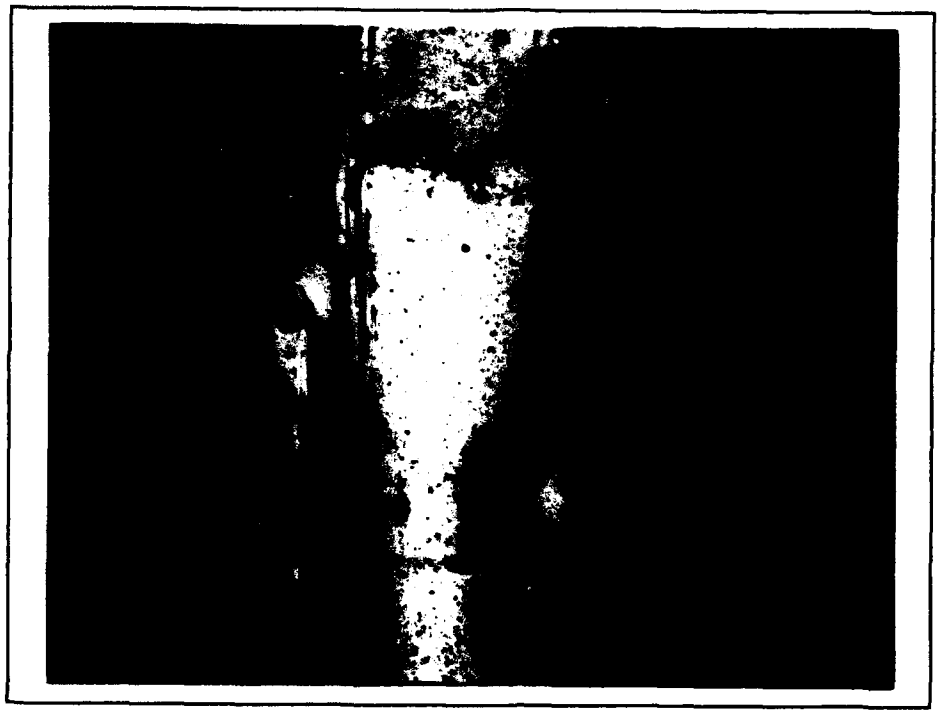

Figure 37. 850° C, ε = 0.000485, x32

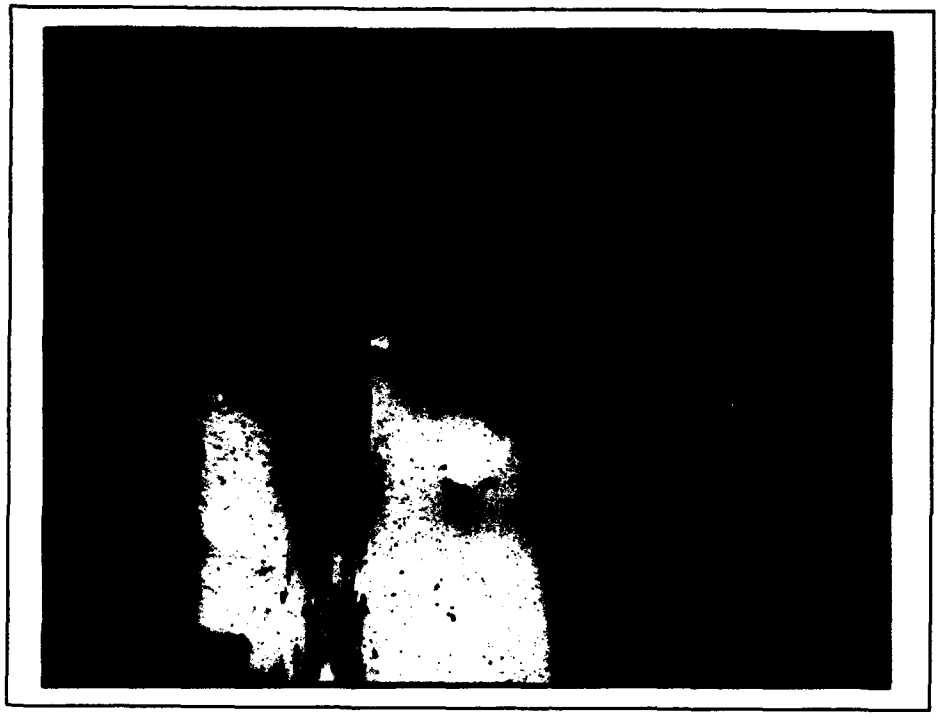

Figure 38. 850° C, ε = 0.000813, x32

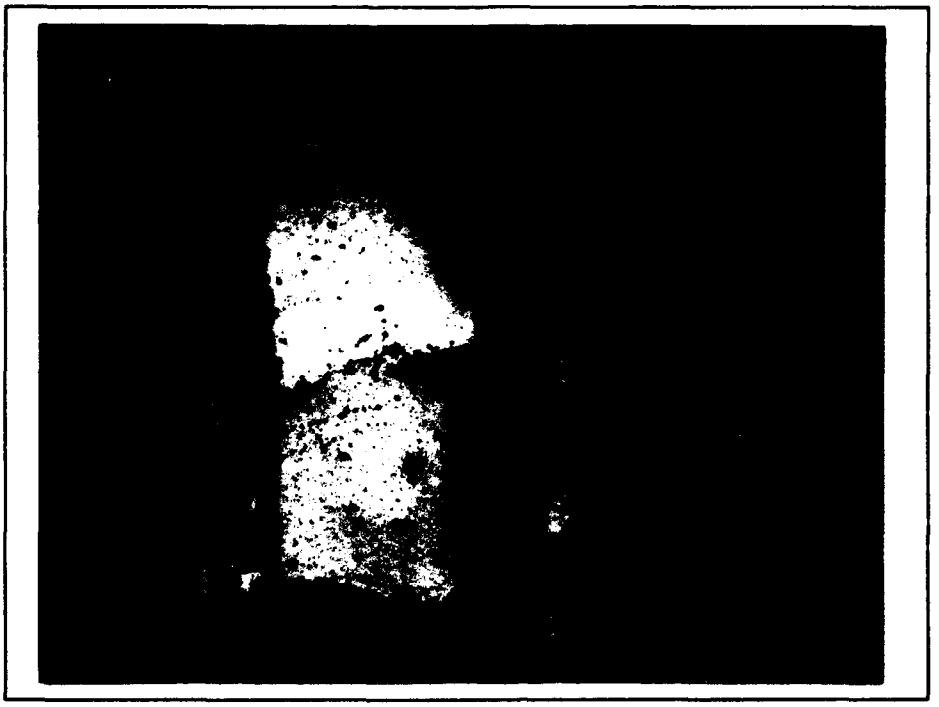

Figure 39. 850° C, ε = 0.00105, x32

photographs (Figures 29, 34 and 39), the central 90° ply region has a lower crack density then the outer 90° plies.

At temperatures above 800° C the interface between the SiC fibers and the CAS matrix begins to show the affects of oxidation. The oxidation results in a brittle layer forming between the fiber and matrix, weakening the interface. This oxidation and resulting debonding at lower strain levels results in greater fiber pull-out at the failure surface. As a result of oxidation, the fiber-matrix interface is weakened, and a greater portion of the load is passed on to the fibers, causing them to fail at a lower strain level. Microphotographs of the fibers of failed specimens show the

affects of oxidation. Figures 40 and 41 show the fibers of the room temperature test specimen. The fibers are clean and undamaged, indicating that the interface has not been affected. Figures 42 and 43 show the fibers of the 700° C test specimen; these fibers are also clean and undamaged. Figures 44 and 45 show the fibers from the 850° C test specimen. Debris on the fibers and variations in the fiber surface indicate oxidation has occurred.

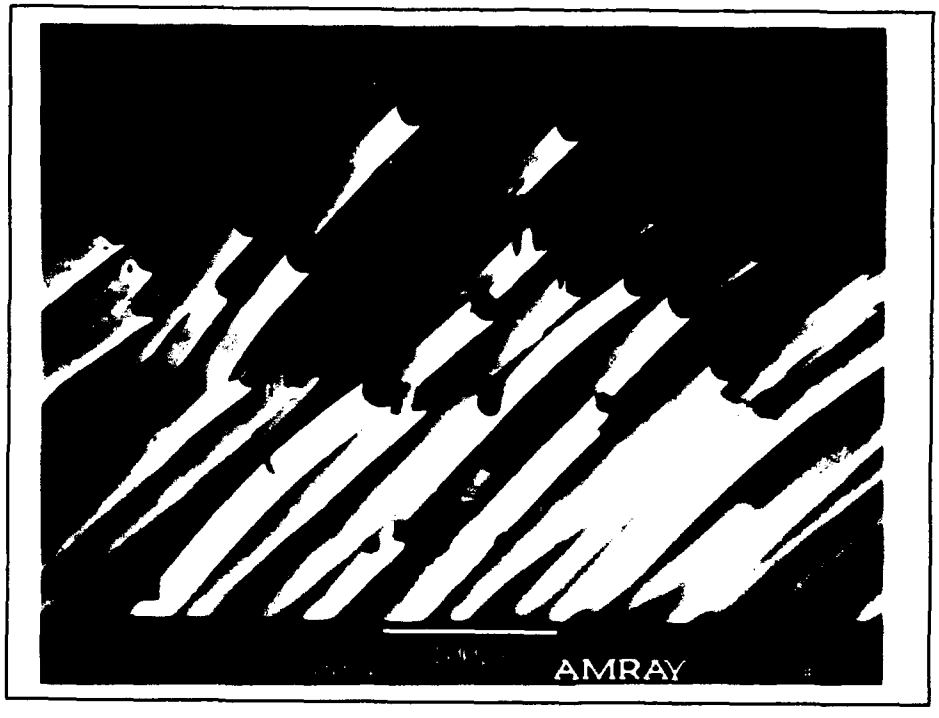

Figure 40. Fractured Fibers of Room Temperature Specimen

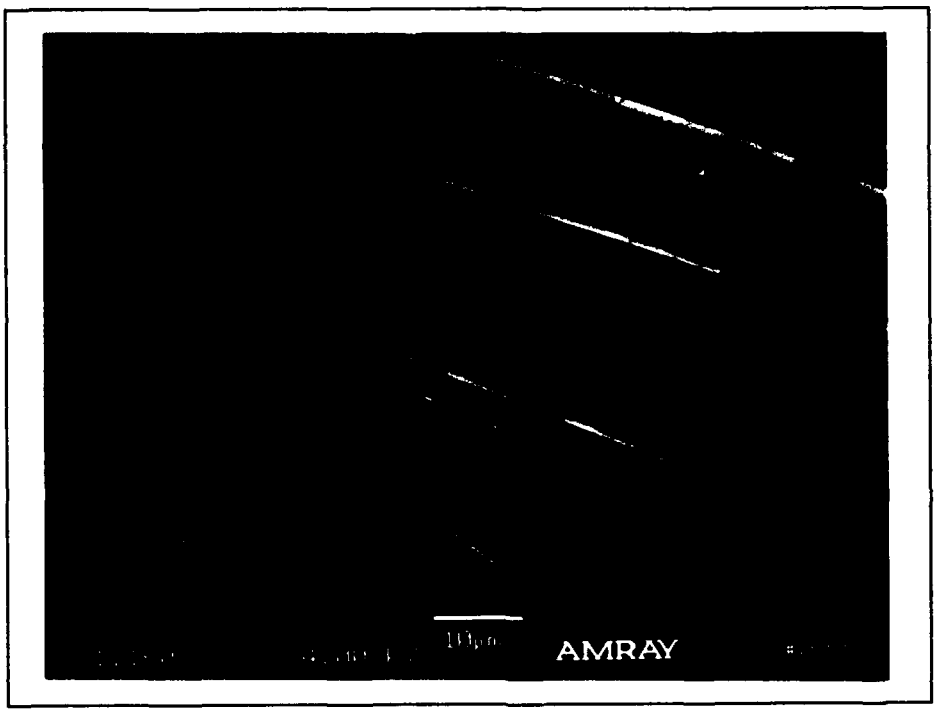

Figure 41. Fractured Fibers of Room Temperature Specimen

Figure 42. Fractured Fibers of 700° C Specimen

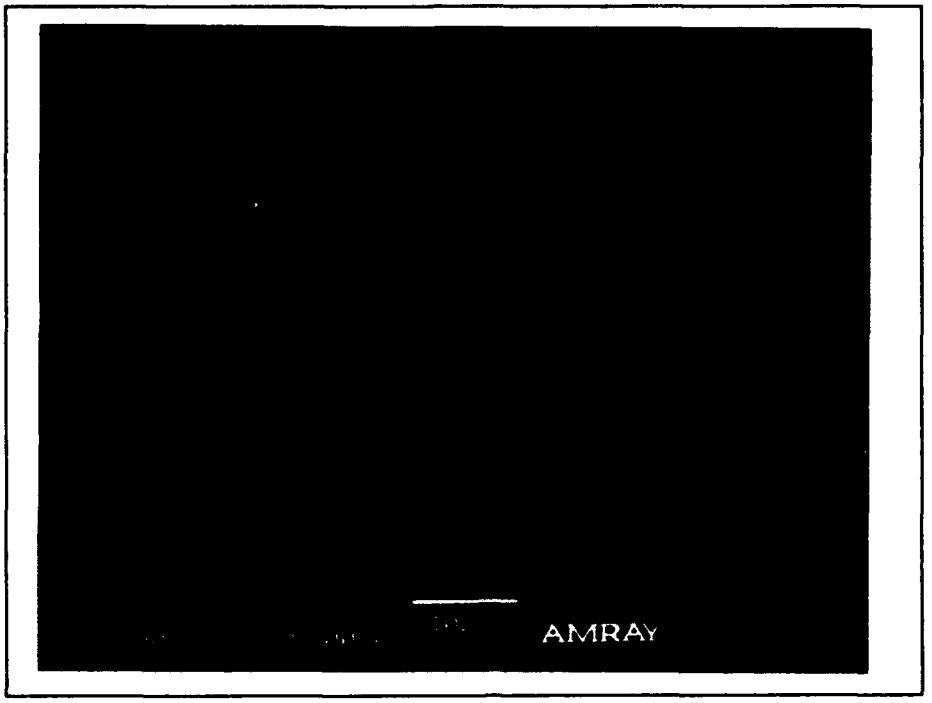

Figure 43. Fractured Fibers of 700° C Specimen

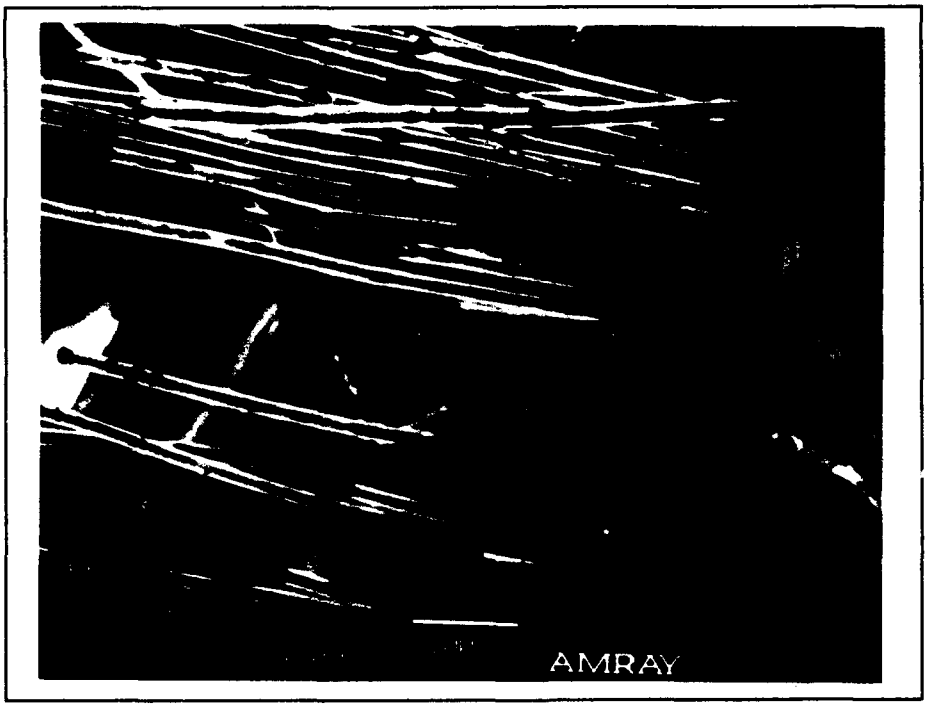

Figure 44. Fractured Fibers of 850° C Specimen

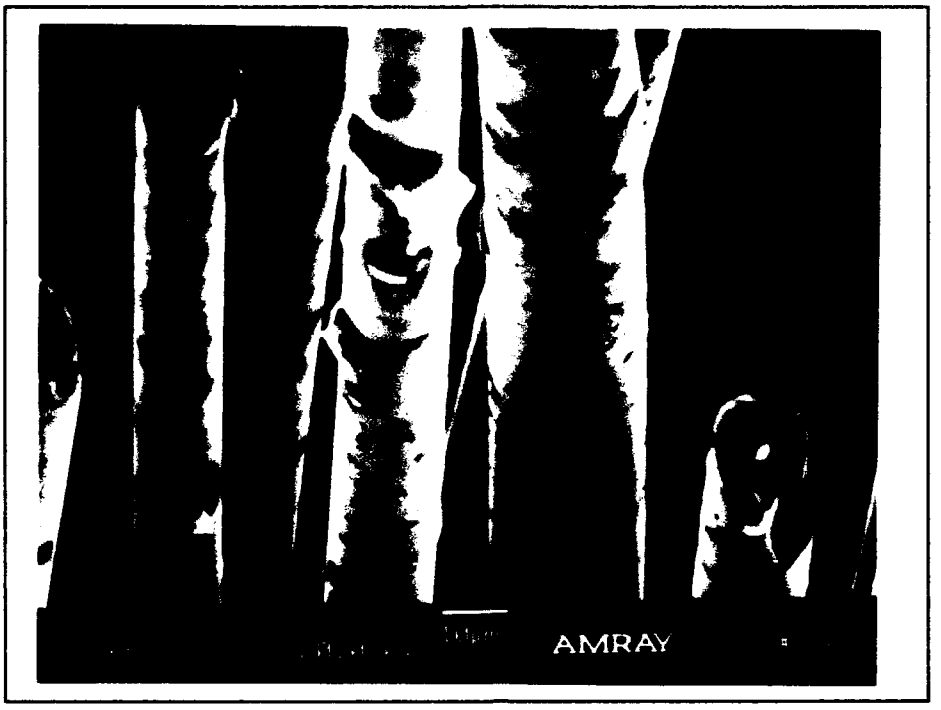

Figure 45. Fractured Fibers of 850° C Specimen

Further investigation of debonding was conducted by sectioning specimens that were tested at each temperature. Using a diamond saw, cross-sections were cut near the failure surface and within the gage length/heated zone. This provided the means to examine the specimen in the direction of loading, versus perpendicular to the direction of loading as in the replica photographs. This was done to enable examination of crack interaction with the matrix and interface of the 0° fibers and matrix. Figure 46 is a microphotograph of a section from a failed room temperature specimen. Crack propagation around the 0° fibers (perpendicular to page) is evident as cracks meeting the

fibers, and either damaging the fibers or moving along part of the interface before continuing through the matrix. No evidence of complete fiber debonding was found. Figure 47 is a microphotograph of a failed 700° C specimen. Crack progression is seen as cracks meeting the fiber and moving along the interface before continuing through the matrix.

Evidence of debonding is seen in Figure 48, a microphotograph of a section taken from a failed 850° C specimen. Cracks are visible in the matrix surrounding the fibers, as well as debonding (dark ring) around the fiber. The interface oxidizes when the cracks in the surrounding matrix allow oxygen to diffuse through the matrix and come into contact with the fiber. Other fibers in the photograph are at different stages of debonding due to variations in matrix cracking and exposure to oxygen.

Thermal cycling tests were conducted to determine the affect of the heating and cooling necessary for the incremental tests conducted to document the damage progression. The results from these tests showed that in all three cases there was no change in crack density or damage progression due to thermal cycling. Figure 52 is the stress-strain response at 700° C, loaded to 40% of expected ultimate strength. The first knee, which was found in the monotonic tests to occur at approximately 40 MPa, is labeled point A. The load level for the test was chosen to be above the first knee to ensure that a significant amount of damage had

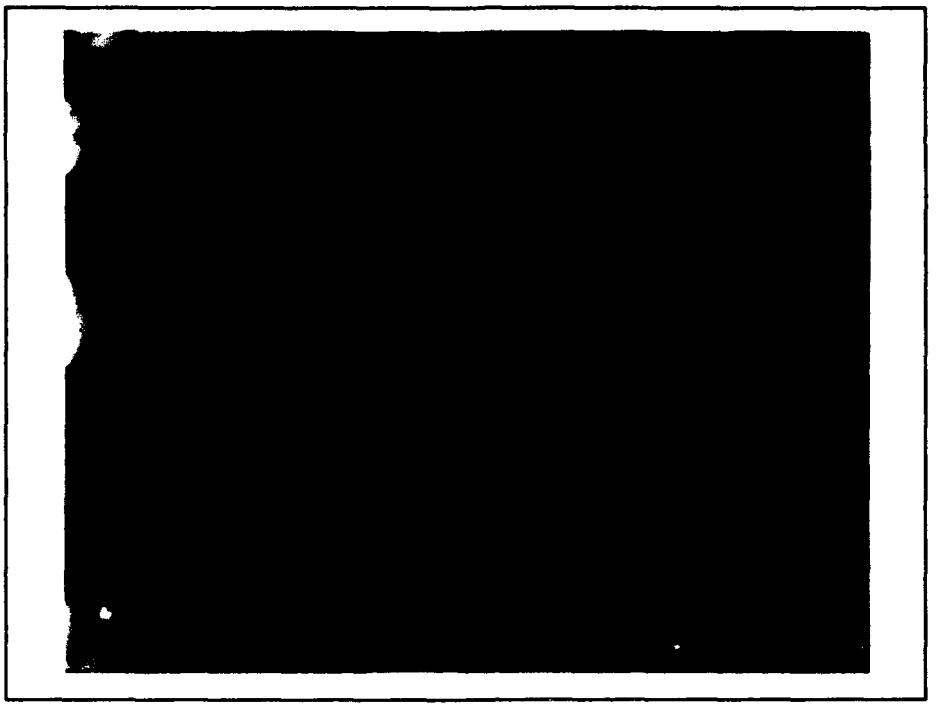

Figure 46. Sectioned Specimen, Room Temperature, x400

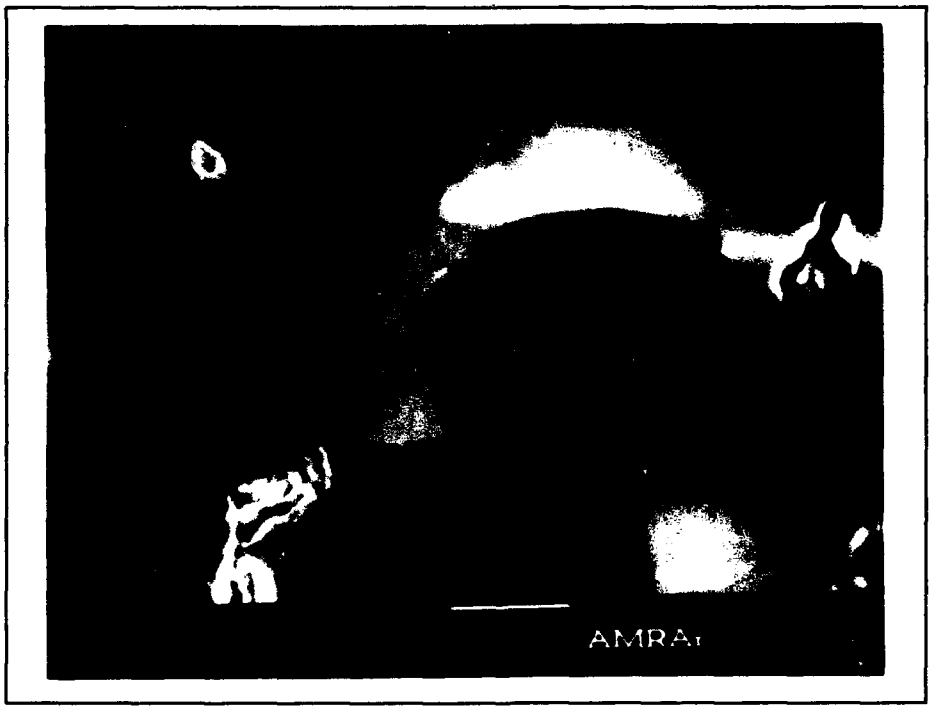

Figure 47. Sectioned Specimen, 700° C, x400

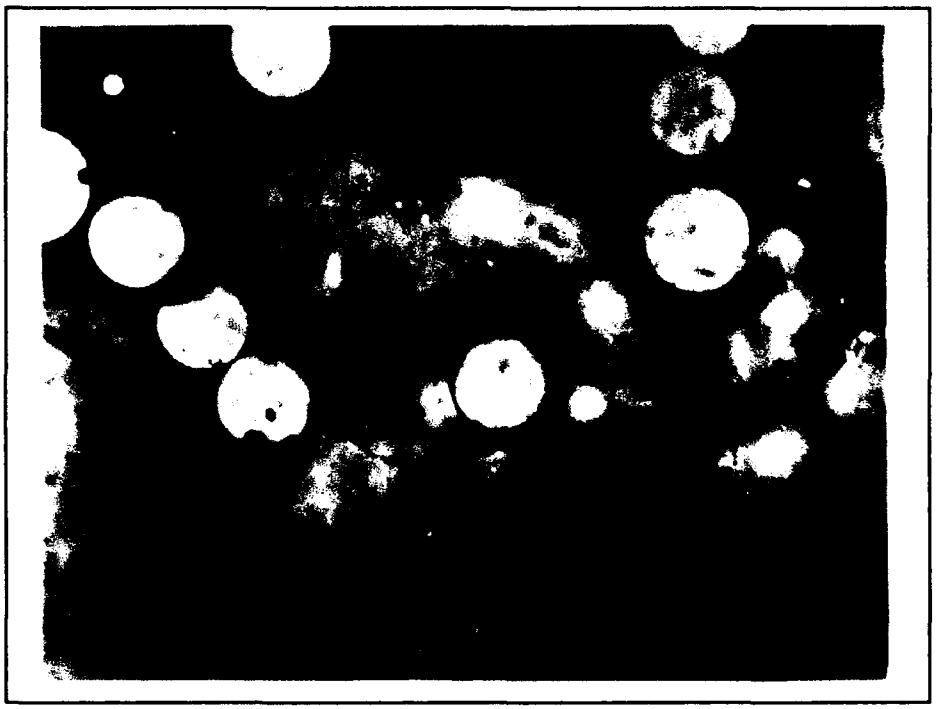

Figure 48. Sectioned Specimen, 850° C, x400

occurred. Figure 53 is the damage after the initial load of 40% of the ultimate strength at 700° C. Figure 54 is the replica after 4 heat cycles, showing no change in damage from the initial cycle. A thermal cycling test was also conducted at 850° C with an initial load of 40% of the expected ultimate strength, and showed no change in damage. Figure 55 is the stress-strain response of a specimen subjected to a load level of 70% of the expected ultimate strength at 850° C. The first knee, which was found to occur at approximately 40 MPa, is labeled point A. Figures 56 and 57 show the replica before and after thermal cycling. There is no change in damage due to four thermal cycles

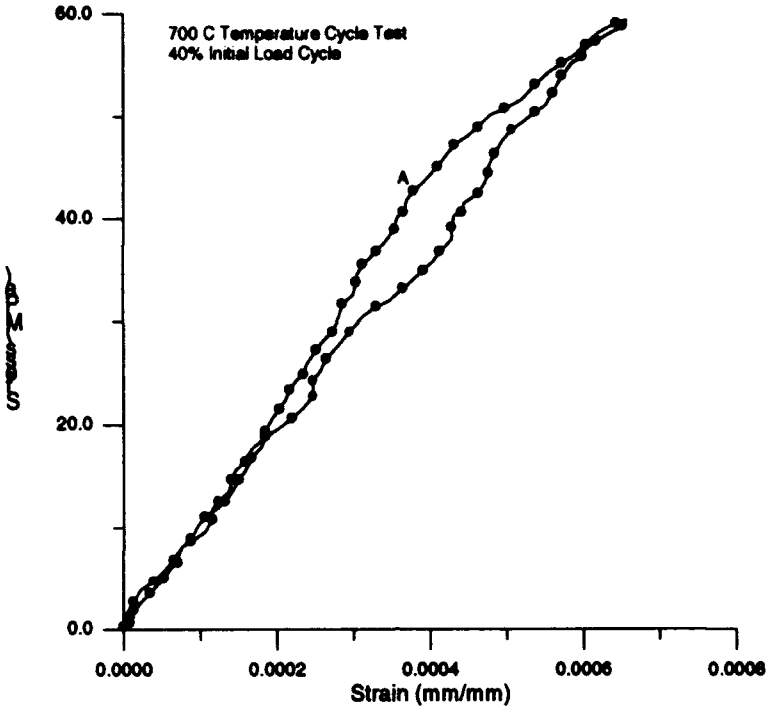

Figure 49. Stress-Strain Response of Specimen at 700° C Tested for Thermal Cycling

Figure 50. Initial Damage, x40

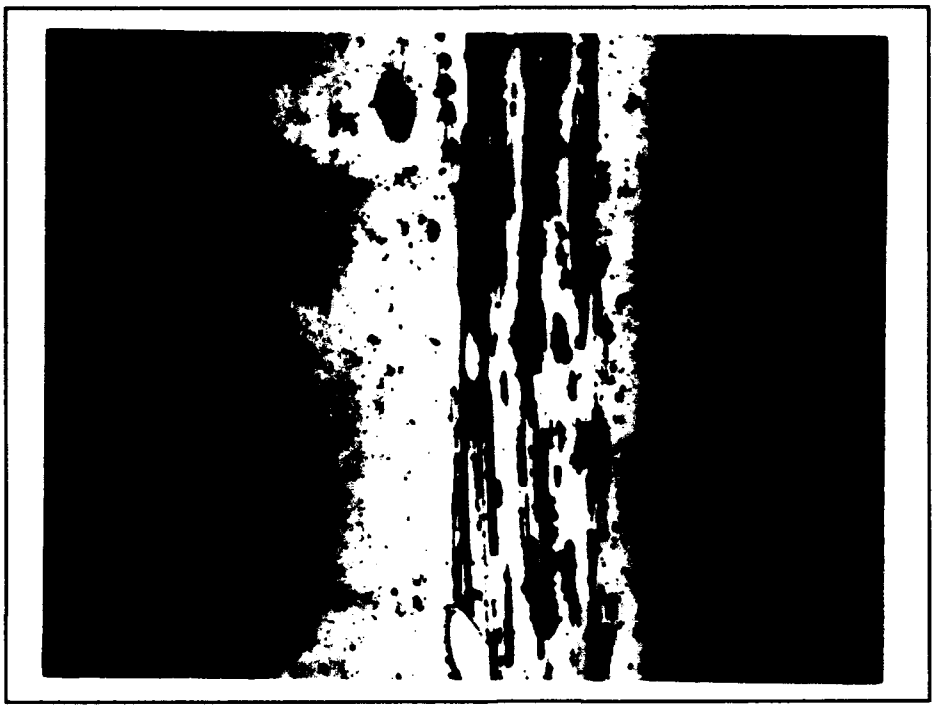

Figure 51. Damage After Four Thermal Cycles, x40

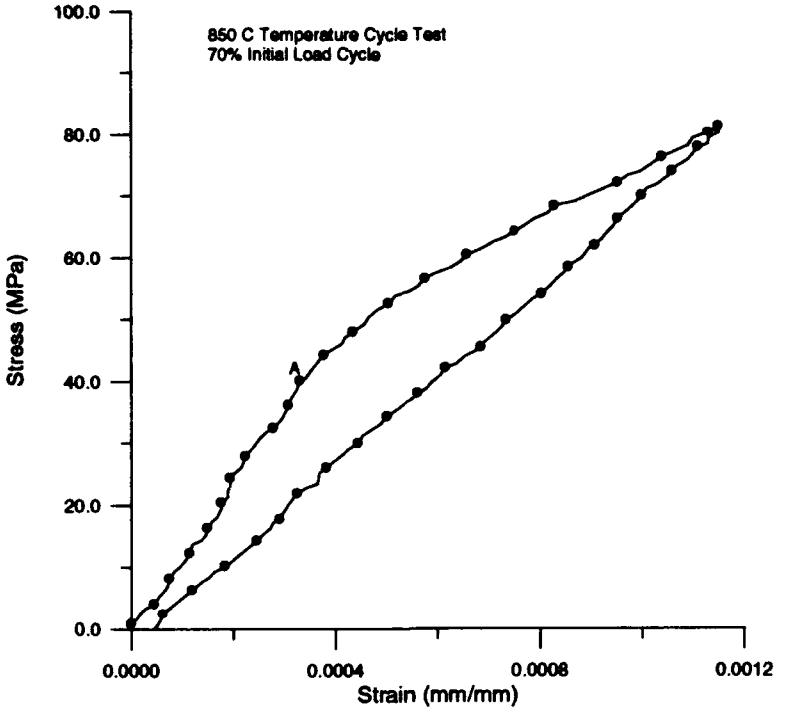

Figure 52. Stress-Strain Response of Specimen at 850° C Tested for Thermal Cycling

Figure 53. Initial Damage, x40

Figure 54. Damage After Four Thermal Cycles, x40

after a specimen was subjected to 70% of the expected ultimate strength at 850° C.

4.5. Failure Surfaces

The failure surfaces of the room temperature and 700° C ultimate tests (Figures 55 - 58) show short fiber pull-out, whereas the 850° C ultimate test (Figures 59 and 60) shows much longer pull-out. The longer pull-out indicates greater debonding of the fiber/matrix interface. As the interface oxidizes, more of the load is carried by the fibers due to the lack of shear stress between the fiber and matrix. When the fibers fail there is no bond with the matrix to resist the pull-out. This is due to the oxidation of the fiber/matrix interface at temperatures above 800° C. The variation in the fiber pull-out over the failure surface in the 850° C test is due to the progression of the fiber oxidation.

4.6. Discussion

The decrease in magnitude of the crack density (Figures 21-23) at the elevated temperatures reflects the decrease in ultimate strength (decrease in damage up to failure) when compared to the room temperature results. The crack densities at the elevated temperatures, compared to room

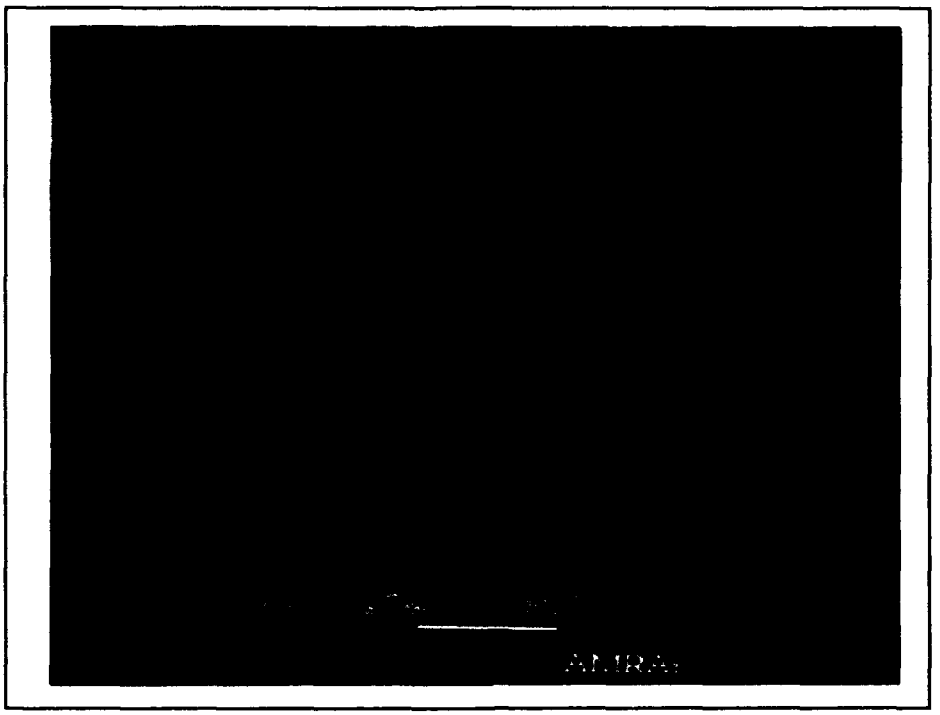

Figure 55. Room Temperature Failure Surface

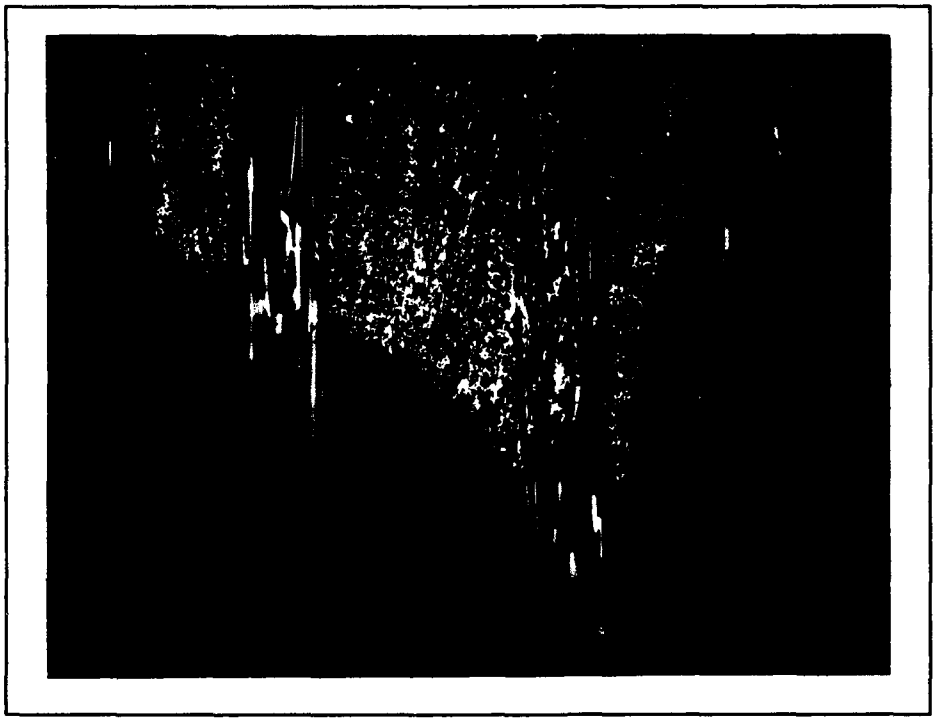

Figure 56. Room Temperature Failure Surface

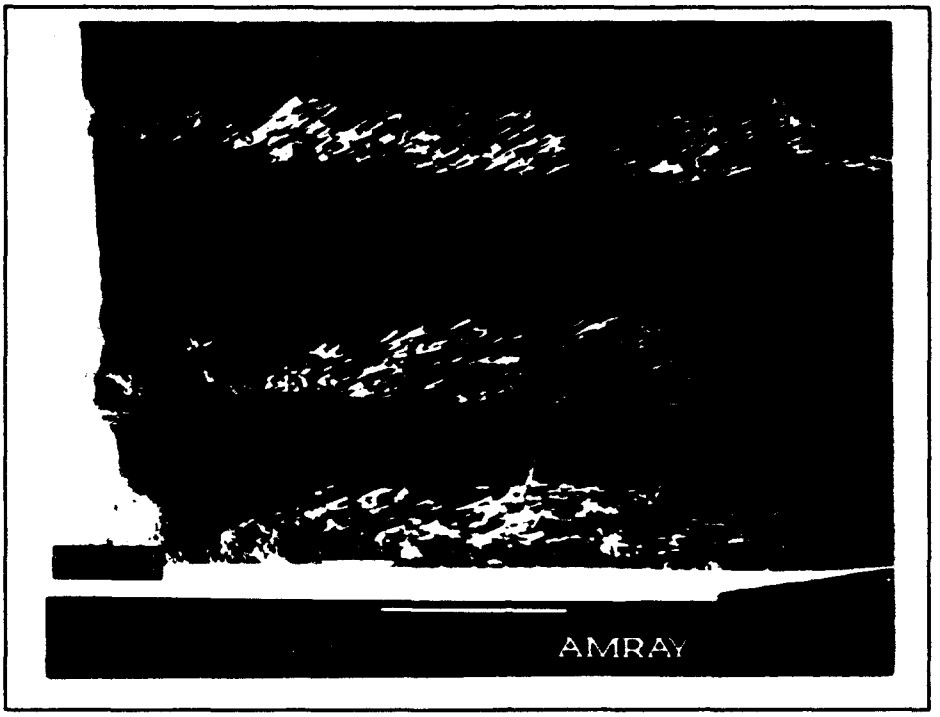

Figure 57. 700° C Failure Surface

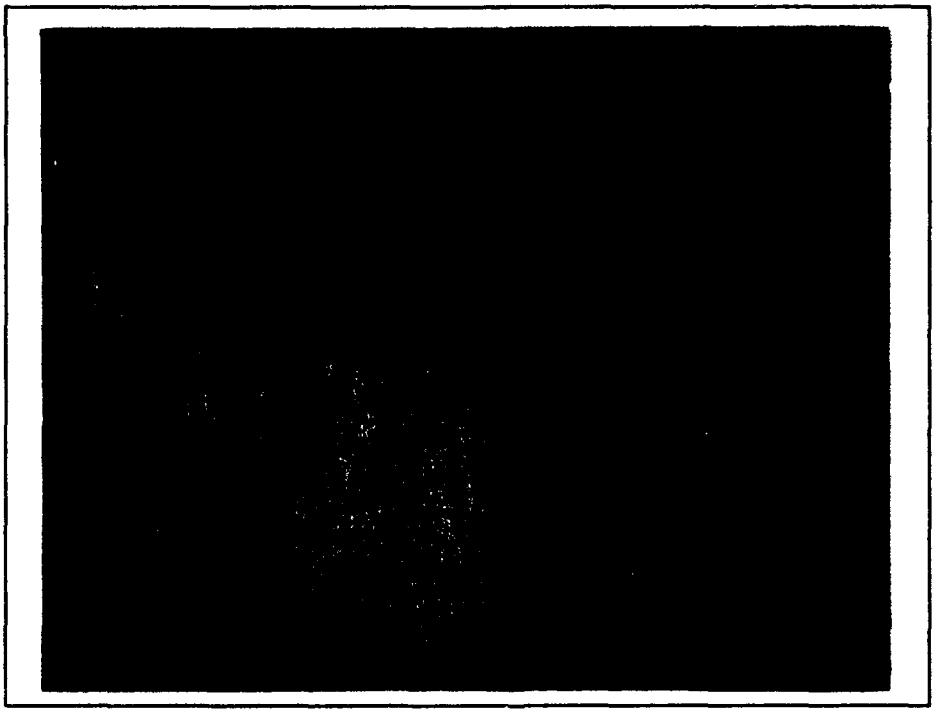

Figure 58. 700° C Failure Surface

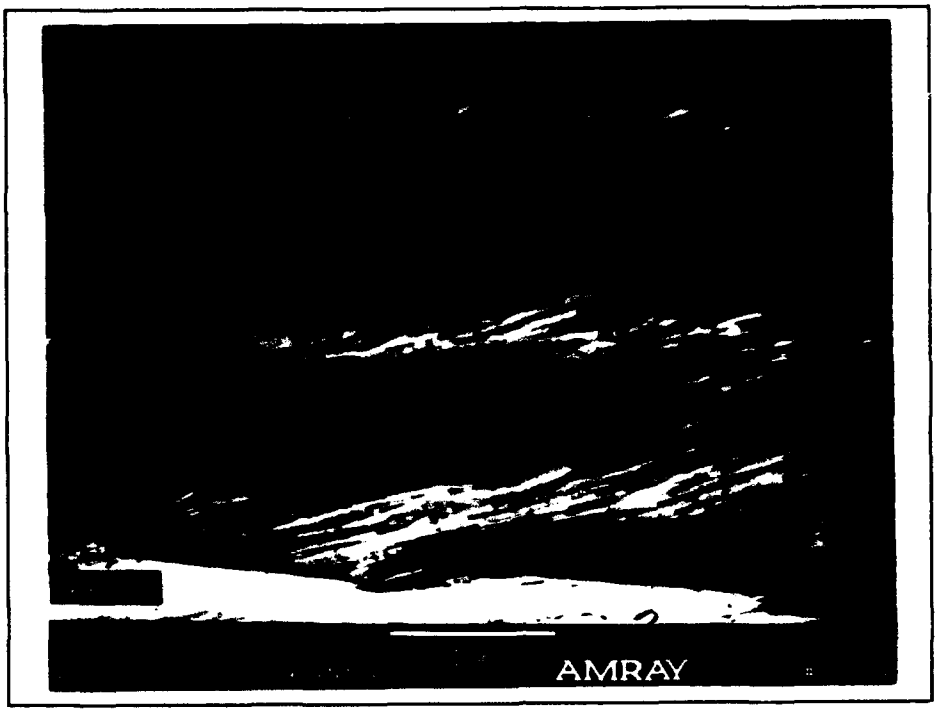

Figure 59. 850° C Failure Surface

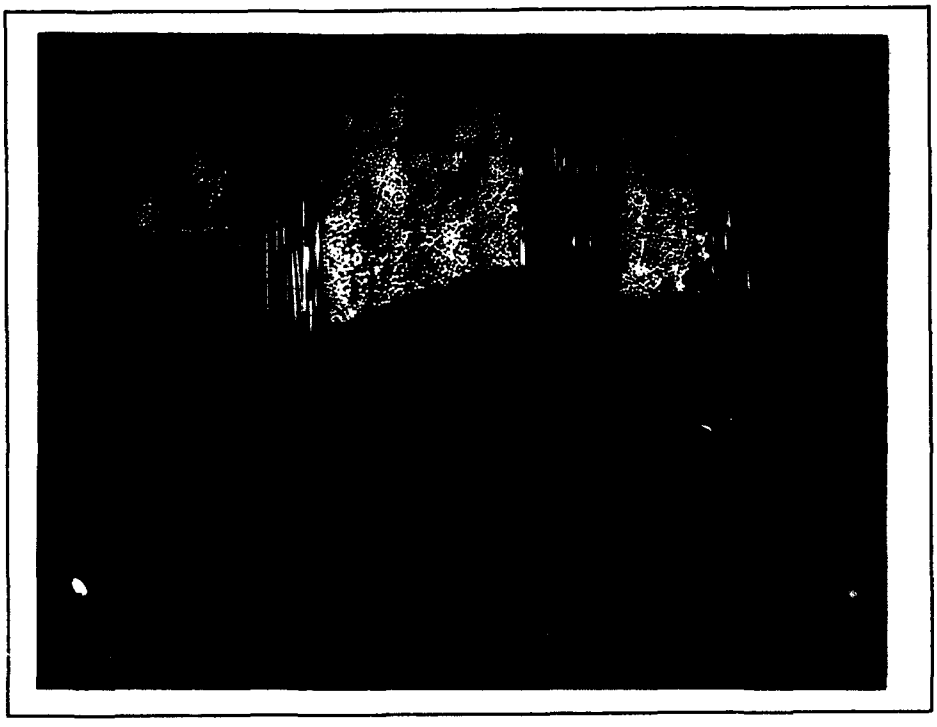

Figure 60. 850° C Failure Surface

temperature, decreased approximately 50% for the 0° plies, and approximately 30% for the 90° plies prior to failure. Comparing the crack density curves for 700° C and 850° C, there is a decrease in crack density at failure in the 0° plies whereas the 90° plies have a similar pre-failure crack density.

At room temperature, cracks initiate in the 90° matrix, then extend across the central 90° plies and also appear in the outer 90° plies. As the applied load, and accompanying strain, increase, the number of cracks increases. The cracks propagate quickly due to the low failure strain of the matrix and weakness of the fiber/matrix bond under transverse loading. Eventually the matrix is unable to carry any of the load (i.e. after the first knee of stress-strain curve). The cracks also begin to propagate into the 0° plies. As the matrix cracks in the 90° plies increase, the portion of the load that they are able to carry is reduced. This unsupported load is carried by the 0° plies. As the load is increased in the 0° plies, the matrix cracks increase in these plies. The fibers and matrix are well bonded, and share the load. Crack propagation is slow due to bridging of the fibers. As with the 90° plies, the matrix eventually fails, leaving only the fibers to carry the load (second knee of stress-strain curve). Many of the cracks that are bridged by fibers eventually cause the fibers to break due to increased strain of the matrix that

is transferred by the fiber/matrix bond. In these tests no cracks were detected parallel to the 0° fibers, which would indicate that delamination had occurred.

At elevated temperatures, the damage progression and crack development begin in the same way. The primary difference is the inability of the 0° matrix to completely transfer the applied load to the 0° fibers after the 90° plies have failed. This inability is due to the oxidation of the fiber/matrix interface, resulting in a weak interfacial bond. The oxidation occurs when cracking of the 90° plies and 0° matrix allows oxygen to diffuse into the material. Since it is dependent on temperature, cracking, and exposure to oxygen, only portions of the interface are weakened. The remainder of the interface, which is unaffected (unoxidized), is able to transfer the load. As fibers break, they are unable to transfer the load to other fibers through the matrix, resulting in a higher load being applied to the remaining fibers. This is shown by the decrease in failure strain of the elevated temperature tests. At lower temperatures, as the 90° plies crack the load can be transferred to the 0° matrix, to be carried by the remaining matrix or transferred to other fibers. As the interface oxidizes at the higher temperatures, portions of the fibers debond, and are unable to transfer the load to the matrix. Other portions are not oxidized or debonded, and are able to maintain or transfer the load.

The first knee of the stress-strain curves occurs between 0.0003 and 0.00035 mm/mm. This strain level corresponds to a substantial increase and roll-off in the crack density of the 90° plies, indicating possible failure of the 90° plies. The second knee occurs between 0.0016 and 0.0018 mm/mm, corresponding to the roll-off of the 0° plies crack density, indicating failure of the 0° matrix.

5. Conclusions

The objective of this study was to investigate the static fracture behavior of a ceramic composite when subjected to tensile loading at elevated temperatures. For this purpose, a cross-ply, $[0/90]_{2s}$, Nicalon/CAS CMC was employed. Tests were conducted at room temperature, 700° C, and 850° C, under monotonically and incrementally increasing loading conditions. Replication was used during the incremental load tests to assess damage initiation and progression. The results from the tests at the three temperatures were compared to determine the affects of the increasing temperature. The conclusions drawn from this study are as follows:

1. The static strength of the material is reduced at elevated temperatures.
2. The crack density prior to failure decreases as the temperature increases.
3. Damage mechanisms are the same at room temperature and 700° C.
4. Fiber debonding resulting from oxidation of the fiber/matrix interface dominates the failure mechanisms at 850° C.

Bibliography

1. Mall, S. and R. Y. Kim. *Failure Mechanisms in Laminates of Silicon Carbide/Calcium-Aluminosilicate Ceramic Composite,* Composites, 23: 215-222 (July 1992).

2. Zawada, L. P., L. M. Butkus, and G. A. Hartman. *Tensile Behavior of Silicon Carbide Fiber-Reinforced Aluminosilicate Glass,* Journal of the American Ceramic Society, 17: 2851-2858 (1991).

3. Harris, B., F. A. Habib, and R. G. Cooke. *Matrix Cracking and the Mechanical Behavior of SiC-CAS Composites,* Proceedings of the Royal Society of London, 437: 109-131 (1992).

4. Karandikar, Prashant, and Tsu-Wei Chou. *Characterization and Modeling of Microcracking and Elastic Moduli Changes in Nicalon/CAS Composites,* Composites Science and Technology, 46: 1-11 (1993).

5. Sorensen, B. F., R. Talreja, and O. T. Sorensen. *Damage Development in a Ceramic Matrix Composite Under Mechanical Loading,* Proceedings of the 5th European Conference on Composite Materials, ECCM-5, 613-618, 1992.

6. Opalski, Frank A. Fatigue Behavior of a Cross-ply Ceramic Matrix Composite Under Tension-Tension and Tension-Compression Loading. MS Thesis, AFIT/GAE/ENY/92D-02, School of Engineering, Air Force Institute of Technology (AU), Wright-Patterson AFB OH, December 1992.

7. Rousseau, Carl Q. *Monotonic and Cyclic Behavior of a Silicon Carbide/Calcium-Aluminosilicate Ceramic Composite,* Thermal and Mechanical Behavior of Metal Matrix and Ceramic Matrix Composites, ASTM SPT 1080.

8. Lee, Shin Steven. Damage Analysis and Mechanical Response of As-Received and Heat-Treated Nicalon/CAS-II Glass-Ceramic Matrix Composites. PhD dissertation. Virginia Polytechnic Institute and State University, Blacksburg, VA, 19XX.

9. Mah, T., M. G. Mendiratta, and others. *High-Temperature Mechanical Behavior of Fiber-Reinforced Glass-Ceramic-Matrix Composites*, Journal of the American Ceramic Society, 68: C248-251 (1985).

10. Stewart, R. L., and others. *Fracture of SiC Fiber/Glass-Ceramic Composites as a Function of Temperature*, Fracture Mechanics of Ceramics, 7: 33-51 (1986).

11. Khobaib, M., and L. Zawada. *Tensile and Creep Behavior of a Silicon Carbide Fiber-Reinforced Aluminosilicate Composite*, Ceramic Engineering and Science Proceedings, 12: 1537-1555 (1991).

12. Prewo, K. M. Advanced Fabrication and Characterization of SiC Fiber Reinforced Glass-Ceramic Matrix Composites, Interim Report, September 15, 1981 - April 30, 1983. ONR Contract N00014-81-C-0571. East Hartford CT: United Technologies Research Center, 24 May 1984.

13. Mah, Tai-Il. *Fiber-Reinforced Ceramic-Matrix Composites*, Proceedings of NASA/DoD Conference on Metal Matrix, Carbon, and Ceramic Matrix Composites. 245-260. 1984.

14. Agarwal, Bhagwan D. and Lawrence J. Broutman. Analysis and Performance of Fiber Composites (Second Edition). New York: John Wiley and Sons, 1990.

15. Bachmann, S. E. Transverse Cracking in a Fiber Reinforced Ceramic Matrix Composite. MS thesis, AFIT/GAE/ENY/90D-2. School of Engineering, Air Force Institute of Technology (AU), Wright-Patterson AFB OH, December 1990.

16. Tuznik, R. Fatigue Behavior of a Cross-Ply Ceramic Matrix Composite at Elevated Temperatures Under Tension-Tension Loading. MS Thesis, AFIT/GAE/ENY/93D-28, School of Engineering, Air Force Institute of Technology (AU), Wright-Patterson AFB OH, December 1993.

December 1993 Master's Thesis

Static Fracture Behavior of a Ceramic Matrix Composite at Elevated Temperatures

David M. Agins, Capt, USAF

Air Force Institute of Technology
Wright-Patterson AFB, OH 45433-6583

AFIT/GAE/ENY/93-1

Dr. Walter Jones
AFOSR/NA
Bolling AFB, DC 20322-6448

This study investigated systematically the damage initiation, damage progression, and failure modes of a ceramic matrix composite, Nicalon/CAS, when loaded in tension at elevated temperatures in the presence of air. A cross-ply lay-up, $[0/90]_{2s}$, was studied. The primary means of analysis were stress-strain data taken during monotonic and incremental load tests and crack density assessments. Testing was conducted at room temperature, 700° C,and 850° C. The stress-strain response was consistent for monotonic and incremental loading, except for a decrease in failure load at the elevated temperatures, Initial damage progression was also consistent, but the damage leading to failure and the final failure mode at 850° C were different due to the oxidation of the fibers. The oxidation created a brittle interface between the fiber and matrix, which resulted in an increase in fiber pull-out at the failure surface.

ceramic, composite, high temperature, fracture, tension 73

Unclassified Unclassified Unclassified UL

December 1993 Master's Thesis

Static Fracture Behavior of a Ceramic Matrix Composite at Elevated Temperatures

David M. Agins, Capt, USAF

Air Force Institute of Technology
Wright-Patterson AFB, OH 45433-6583

AFIT/GAE/ENY/93-1

Dr. Walter Jones
AFOSR/NA
Bolling AFB, DC 20322-6448

APPROVED FOR PUBLIC RELEASE; DISTRIBUTION UNLIMITED.

This study investigated systematically the damage initiation, damage progression, and failure modes of a ceramic matrix composite, Nicalon/CAS, when loaded in tension at elevated temperatures in the presence of air. A cross-ply lay-up, $[0/90]_{2s}$, was studied. The primary means of analysis were stress-strain data taken during monotonic and incremental load tests and crack density assessments. Testing was conducted at room temperature, 700° C,and 850° C. The stress-strain response was consistent for monotonic and incremental loading, except for a decrease in failure load at the elevated temperatures, Initial damage progression was also consistent, but the damage leading to failure and the final failure mode at 850° C were different due to the oxidation of the fibers. The oxidation created a brittle interface between the fiber and matrix, which resulted in an increase in fiber pull-out at the failure surface.

ceramic, composite, high temperature, fracture, tension 73

Unclassified Unclassified Unclassified UL